Supporting information

Formation of Secondary Brown Carbon in Biomass Burning Aerosol Proxies through NO_3 Radical Reactions

Chunlin Li,[†,∇] Quanfu He,[†,∇] Anusha Priyadarshani Silva Hettiyadura,[‡] Uwe Käfer,[§,∥] Guy Shmul,[⊥] Daphne Meidan,[†] Ralf Zimmermann,[§,∥] Steven S. Brown,[#,★] Christian George,[◆] Alexander Laskin,[‡] and Yinon Rudich[*,†]

[†]Department of Earth and Planetary Sciences, Weizmann Institute of Science, Rehovot 76100, Israel

[‡]Department of Chemistry, Purdue University, West Lafayette, Indiana 47907, United States

[§]Joint Mass Spectrometry Centre, University of Rostock, Dr.-Lorenz-Weg 2, 18059 Rostock, Germany

[∥]Joint Mass Spectrometry Centre, Cooperation Group "Comprehensive Molecular Analytics" (CMA), Helmholtz Zentrum München, Ingolstadter Landstrasse 1, 85764 Neuherberg, Germany¨

[⊥]Department of Chemical Research Support, Weizmann Institute of Science, Rehovot 76100, Israel

[#]Chemical Science Division, NOAA Earth System Research Laboratory (ESRL), Boulder, Colorado 80305, United States

[★]Department of Chemistry, University of Colorado, Boulder, Colorado 80309-0215, United States

[◆]Univ Lyon, Université Claude Bernard Lyon 1, CNRS, IRCELYON, F-69626, Villeurbanne, France

[∇]Contributed equally

[*]Email: yinon.rudich@weizmann.ac.il

Supporting Information consists of 31 pages, including 13 figures, 6 tables and 6 text sections.

Content:

S1. Wood Tar Aerosol Generation. Detailed procedures for generation of wood tar aerosol can be found elsewhere.[1,2] In short, 100 g commercial wood pellets (Hallingdal Trepellets, water content 7-8 wt.%, 2-3 cm in length, 8 mm in diameter) were smashed, and dry distillated at 550 °C in a flask combustor equipped with electric heating plate and with controlled high-purity N_2 supply of 1.5 L min^{-1}. Wood tar material in the pyrolysis emissions was collected using a water-cooled condensation system (15 °C for cycling water). The collected viscous wood tar materials were concentrated by heating to 300 °C under high-purity N_2 atmosphere. The concentrated tar solution was extracted using ultrapure MiliQ water (18.2 MΩ, UV sterilized), acetonitrile, and a mixture of dichloromethane/hexane (1:1, *v/v*). All the extracted samples passed through syringe filters with 0.2 μm Teflon membrane (Pall Life Science) to filter impurities and particulates. The dichloromethane/hexane extract fractions were dried via rotatory evaporation (water bath at 50 °C) and re-dissolved in a mixture of acetonitrile and methanol (1:1, *v/v*). The extracts obtained with the solvents of water, acetonitrile, and organo-mixture of dichloromethane/hexane are hereafter referred to as polar, moderately polar, and nonpolar wood tar, respectively. All the solvents (e.g., acetonitrile, methanol, dichloromethane, and hexane) were used as received with HPLC grade and purity≥99.9% (Sigma-Aldrich).

Following extraction, a constant output atomizer (Model 3076, TSI) was used to nebulize the wood tar solutions with high-purity N_2 at 15-20 psi pressure. A splitter delivered 0.8 L min^{-1} of the aerosols to a quartz heating tube (*L*:20 cm, *ID*: 0.7 cm, maintained at 300 °C, residence time ~0.6 s), through which wood tar aerosols were dehydrated and compacted, mimicking heat shock in the fire for burning released particles. Two activated charcoal and one silica gel denuders (*L*:70 cm, *ID*: 7 cm) in series were fixed downstream, for removing the solvents in both gas and particulate phases. With this procedure, we generated wood tar particles with different chemical polarities.

S2. Aerosol Flow Tube Reactor (AFR). The flow reactor was a cylindrical glass tube of 7.5 cm inner diameter and length of 72 cm. The input port of the reactor was a conical mixing section fitted with three separated inlets, of which one inlet was connected downstream of the atomizer system for introduction of the particles, the other two inlets were used to supply O_2 and N_2O_5. Prior to experiments, the flow tube was cleaned with N_2 and high concentration of O_3 until no particles were detected using a condensation particle counter (CPC, Model 3775 low, TSI). During the experiments, a stable flow of the conditioned wood tar particles at 0.8 L min^{-1} was introduced into the AFR and mixed with 0.2 L min^{-1} oxygen (purity of 99.999%). A flow of gaseous N_2O_5 with N_2 as carrier gas at 0.06-0.10 L min^{-1} was added as a source of NO_3 radicals ($N_2O_5 \leftrightarrow NO_2 + NO_3$) to oxidize wood tar particles in the presence of NO_2 and O_2 at room temperature (296.5 ± 0.5 K) in the dark. A laminar flow (Reynolds number < 23.5) of total 1.0-1.1 L min^{-1} with a residence time (RT) of approximately 165 s was achieved in the AFR. Three more charcoal denuders (*L*:70 cm, *ID*: 7 cm) in series were fixed downstream the flow reactor to adsorb the extra NOx and gases that evaporated from the particles before the wood tar aerosols were characterized. A final N_2 flow of 1.0-1.5 L min^{-1} was supplied to dilute the particles flow. To minimize loss of particles and gases in experiments, conductive rubber tubing was used for the aerosol flow, Teflon tubes and Teflon-made connectors were used to introduce and carry gases.

S3. Generation of NO_3 Radicals and NO_3-N_2O_5 Detection. Dry N_2O_5 crystals were prepared as NO_3 radical reservoir prior to the experiments. Briefly, a flow of NO (≥99.9 %, Verdichtetes Gas) is mixed with ultrahigh purity O_2 (≥99.999%, Air Liquid UK Limited.) in a glass bulb to produce NO_2. The NO_2 reacts with O_3 in a Teflon tube connected to a glass bulb. Ozone is generated online with an ozone generator (Pacific Ozone Tech, USA). The produced N_2O_5 is trapped as white solid flakes in a glass crytotrap which is kept in a mixture of ethanol and dry ice (approximately at -72 °C, cold enough to trap N_2O_5 but not O_3 or NO_2). The reactions taking place are:

$$2NO + O_2 \rightarrow 2NO_2 \quad \text{S1}$$

$$NO + O_3 \rightarrow NO_2 + O_2 \quad \text{S2}$$

$$NO_2 + O_3 \rightarrow NO_3 + O_2 \quad \text{S3}$$

$$NO_3 + NO_2 \overset{k_{eq}}{\leftrightarrow} N_2O_5 \quad \text{S 4}$$

In the experiments, gaseous N_2O_5 was eluted gently from the cold-trap by a small ultrapure N_2 flow followed by mixing with predefined aerosol flow (1.0-1.1 L min^{-1}) in the AFR. NO_3 radicals from N_2O_5 thermal decomposition initiated heterogeneous reactions with the particles. Only Teflon tubes and connectors were used to carry N_2O_5 before mixing with particles. The NO_3 radical oxidation degrees of wood tar particles depend on initial the N_2O_5 mixing ratios which were mediated by controlling the N_2 flow through the cold-trap (60, 80, and 100 sccm, respectively).

N_2O_5 was detected following thermal dissociation by a cavity ring-down spectrometer (CRDS) which has been developed in our group.[3-5] Application of CRDS for NO_3 detection has been extensively described.[6] In short, CRDS consists of a single-wavelength laser light and an optical cavity, the light is modulated and introduced into the optical cavity, two high-reflectivity concave mirrors are mounted at both ends of the cavity to form a stable optical resonator. The light in the cavity bounces back and forth, the decay time of light intensity changes due to gases or/and particles absorption and scattering. The extinction coefficient (α_{ext}) can be directly measured from the light decay time for empty cavity (τ_0) and gases or/ and particle filled cavity (τ), as given in Equation S5:

$$\alpha_{ext} = \frac{L}{lc}\left(\frac{1}{\tau} - \frac{1}{\tau_0}\right) \quad \text{S 5}$$

where L is the optical length, and l is effective cavity length, c is light velocity (2.998×10^8 m s^{-1}). With the known absorption cross section (σ_{abs}) for the specific gas dispersed across the cavity, its concentration (C) can be calculated based on Equation S6:

$$C = \frac{\alpha_{ext}}{\sigma_{abs-NO_3}} \quad \text{S 6}$$

N_2O_5 is measured as NO_3 radical following thermal dissociation at 85 °C, at the NO_3 radical characteristic absorption at 662 nm ($\sigma_{abs-NO3}$ = $(2.23\pm0.35)\times10^{-17}$ cm^2 $molec^{-1}$).[6] The CRDS is equipped with this single-wavelength laser light (HL6545MG, Thorlabs Inc., NJ, USA) with output power of approximately 150 mW. Light decay is measured by a photomultiplier tube (PMT, H10721-20, Hamamatsu Photonics K.K., Hamamatsu, Japan) at a rate of 10-100 MHz. The cavity consists of a temperature-controlled Teflon-made tube (Length: 0.979 m, ID: 0.8 cm) which is kept at 85 °C to avoid wall loss of NO_3 radicals and also to promote thermal composition of N_2O_5. The CRDS has a detection limit of ~ 0.2 pptv (2σ) with integration time of 60 s.

The ring-down constant time in the absence of NO_3 radical was measured by titrating NO_3 radical with NO:

$$NO_3 + NO \rightarrow 2NO_2 \quad \text{S 7}$$

Titration reaction of NO_3 radical occurred in a long Teflon tube (L: 3.0 m, ID: 6.0 mm) upstream of the CRDS. The Teflon tube and the CRDS cavity were maintained at 85 °C. Titration reaction in the long Teflon tube lasted approximately 15 s, which was long enough to reach equilibrium. At fixed N_2O_5 flow (60-100 sccm), the mixing ratio of NO was increased slowly until the residual NO_3 radical concentration was less than 10 times of the detection limit from the CRDS measurement. Based on NO concentration and dilution ratio, the N_2O_5 concentration could be calculated. Note that this refers to the N_2O_5 concentration from the cold-trap, considering dilution. The initial gaseous N_2O_5 mixing ratios in the AFR were 455.1 ± 100.6, 635.7 ± 140.6, and 803.6 ± 177.7 ppbv, corresponding to 60, 80, 100 sccm eluting flow, respectively.

S4. Broadband Complex Refractive Index Retrieval. The processed wood tar particles were first size-selected using an aerodynamic aerosol classifier (AAC, Cambustion, UK). The aerodynamic monodispersed tar particles (D_{aero}) were then scanned by a scanning mobility particle sizer (SMPS, classifier Model 3080, DMA Model 3081, CPC Model 3775 low, TSI) to get their median mobility diameter (D_m). Assuming homogeneous chemical nature and spherical shape for wood tar aerosol (verified via electron microscopy), the particulate effective density (ρ) was calculated by Equation S8:

$$\rho = \frac{D_{aero}}{D_m} \times \rho_0 \qquad \text{S 8}$$

where ρ_0 is unit density of 1.0 g cm^{-3}.

Based on the known effective density, wood tar particles in mobility size range of 175-375 nm with a step of 25 nm were size-selected via AAC in sequence. The size-specific particles were introduced into the dual-channel broadband cavity enhanced spectrometer (BBCES) for light extinction (α_{ext}) measurements in the wavelength of 315-355 and 380-650 nm (at a resolution of 0.5 nm). Particles were size-selected using AAC rather than DMA to avoid the influence of multiply charged particles.[7,8] The α_{ext} of monodisperse particles is determined as the difference in light intensity between a filled cavity and particle-free cavity, taking into account the mirror reflectivity and the Rayleigh scattering of the carrier gas (zero air).[9,10] Setup and operation of the BBCES have been described in He et al.[3] Only a brief description was mentioned here.

A broadband laser-driven white-light lamp (EQ-99CAL LDLS, Energetiq Tech., Inc., MA) equipped with air-cooling and water-circulation cooling system is the light source. The light from the lamp ranges from 170 to 2100 nm and is coupled to a multimode optical quartz fiber of 1mm core (Energetiq). The deep UV region of the light (λ<294 nm) is removed through a long-pass filter (10CGA-295, Newport Corp., CA). A dichroic beamsplitter (400 nm, Dichroic long pass filter, Edmund Optics Inc., NJ) is employed to reflect 315-365 nm light into the first optical cavity (BBCES$_{UV}$). Light with wavelength longer than 380 nm is optically filtrated using bandpass filters (FineNine Optic Technologies, Inc., CA) and reflected into the second cavity (BBCES$_{vis}$). The coupled light is collimated through the dual channels. Each cavity consists of two 2.5 cm, 1 m radius curvature mirrors (FiveNine Optics, USA). The high light reflectivity of the mirrors ensures minor loss varies from 90 to 500 ppm within the wavelength range of 380-650nm. After exiting the cavity, the light is directly collected using a 0.1 cm F/2 fiber collimator (74-UV, Ocean Optics, Dunedin, FL, USA) into one lead of a two-way 100µm core HOH-UV-VIS bundle fiber (SROPT-8015, Andor Technology, Belfast, UK) that is linearly aligned along the input slit of the grating spectrometer. The spectra are acquired using a 163 mm focal length Czerny-Turner spectrometer (Shamrock SR-163, Andor Technology, Belfast, UK) with a charge coupled device (CCD) detector (DU920P-BU, Andor Technology, Belfast, UK) maintained at -50 ºC. The spectrometer is temperature-controlled at 22.0±0.1 ºC. Dark spectra are acquired with the input shutter (SR1-SHT-9003, Andor Technology, Belfast, UK) closed prior to each set of spectra. The wavelength is calibrated using a Hg/Ar pen-ray lamp.

The general expression that relates the extinction coefficient (α_{ext}, in cm^{-1}) of sample particles in an N_2 or air-filled cavity, to the change in intensity of the transmitted light is given in Equation S9:

$$\alpha_{ext}(\lambda, D_m, RI) = R_L\left(\frac{1-R(\lambda)}{d} + \alpha_{Rayleigh}(\lambda)\right)\left(\frac{I_0(\lambda)-I(\lambda)}{I(\lambda)}\right) \qquad \text{S 9}$$

Where R_L is the ratio of the total length to the filled length of the cavity, $R(\lambda)$ is the mirror reflectivity, $\alpha_{Rayleigh}(\lambda)$ is the extinction coefficient due to Rayleigh scattering by N_2 or air, $I_0(\lambda)$ is the spectrum (i.e., the wavelength-dependent intensity transmitted through the cavity and detected by the CCD) of N_2 or air, $I(\lambda)$ is the spectrum with particles and gases present.

Mirror reflectivity of $R(\lambda)$ can be calculated using reference pure gases (e.g., N_2, He, CO_2) with known wavelength-dependent extinction coefficients, taking N_2 and He as reference gases, in Equation S10:

$$\frac{1-R(\lambda)}{d}=\frac{I_{N_2}(\lambda)\times\alpha_{Rayleigh-N_2}(\lambda)-I_{He}(\lambda)\times\alpha_{Rayleigh-He}(\lambda)}{I_{He}(\lambda)-I_{N_2}(\lambda)} \quad \text{S10}$$

Together with the α_{ext} measurement, number concentration of these size-specific particles was monitored with a condensation particle counter (CPC, Model 3775 low, TSI) in parallel with BBCES. Thus, the size-specific particle extinction cross section (σ_{ext}) can be calculated by Equation S11:

$$\sigma_{ext}(\lambda,D_m,RI)=\frac{\alpha_{ext}(\lambda,D_m,RI)}{N_p} \quad \text{S11}$$

where λ is the incident light wavelength (nm).

For spherical and homogeneous particles, RI at each wavelength can be retrieved by minimizing the expression in Equation S12:

$$\chi^2(\lambda)=\sum_{i=1}^{N_{Dm}}\left(\frac{\sigma_{ext,measured}(\lambda)-\sigma_{ext,calculated}(\lambda)}{\sigma_{ext,measured}(\lambda)}\right) \quad \text{S12}$$

Where N_{Dm} is the number of diameters measured and $\sigma_{ext,measured}$ is the theoretical optical cross section calculated based on Mie-Lorenz scattering theory by varying the real and imaginary parts (n and k) of the complex RI. The wood tar particles were size-selected by the AAC based on the aerodynamic motion without charging, hence it avoids the contribution of multiply charged particles, generating highly monodisperse particles and reducing the errors associated with multiply charged large particles.[7,8]

A single-wavelength photoacoustic-cavity ring down spectrometer (PAS-CRDS) was used to directly measure both absorption coefficient (α_{abs}) and extinction coefficient (α_{ext}) at λ=404nm. A diode laser (110 mW, iPulse, Topica Photonics, Munich, Germany) was used as light source, and the laser beam was split into two separate optical paths entering into the multi-pass PAS cell and cavity. In the PAS, modulated laser light is absorbed by gases or/and particles, generating a modulated acoustic wave whose intensity is proportional to the energy absorbed by the sample. The acoustic wave is recorded by a sensitive microphone, which has a characteristic radial and longitudinal resonance when the light source is modulated at the cavity resonance frequency. The specific resonance frequency of the system is found by producing white noise using a speaker in the reference resonator. The PAS calibration procedure is described in our previous work.[9] In short, we used standard particulate nigrosin dye with defined RIs, size, and concentration to construct an operational function between dry particle absorption coefficients and PAS signals. The RI retrieval method is the same as Equation S12. The retrievals have been validated by measuring standard samples and materials, e.g., ammonium sulfate ($(NH_4)_2SO_4$), polystyrene latex (PSL), soot, humic-like substance (HULIS), etc, referring to our previous work.[4,11-13]

S5. Wood Tar Aerosol Chemical Composition Measurements. The fresh and NO_3 radical processed wood tar aerosols were characterized in chemical transformation via both *in situ* and offline techniques.

S5.1. HR-ToF-AMS was applied to monitor the bulk non-refractive composition of wood tar particles online. The mass spectra were acquired in both the high-sensitivity V- and high-resolution W-modes. The vaporizer temperature was set at about 600 ºC, and electron-ionization energy was 70 eV. The data was analyzed using the Squirrel v 1.16A and PIKA v 1.57 codes (http://cires.colorado.edu/jimenez-group/ToFAMSResources/ToFSoftware/). All the organic ions were classified into five groups as C_xH_y (including C_x), C_xH_yO, $C_xH_yO_z$ (H_xO_y, CO, and CO_2 included), $C_xH_yO_iN_p$, and NO_y based on their elemental compositions, where x, y, p≥1, i≥0, and z≥2. Mass spectrum was processed from V-mode results, and elemental analyses to determine the molar elemental ratios (C/O, H/O, and N/O) and mass ratio

of organic matter to organic carbon (OM/OC) were based on W-mode results.[14]

S5.2. Individual particle analysis. The particles collected on polycarbonate membranes were imaged using a Quattro Environmental scanning electron microscopes (ESEM, Thermoscientific Quattro S), and semi-quantitative elemental compositions (O, C, N, and S) of these particles were acquired from the energy-dispersive X-ray analysis (EDX).

S5.3. Vibrational spectroscopy measurements. The characteristic functional groups of wood tar aerosols were measured using an FT-IR (Thermo Scientific Nicolet™ 6700). To moderately polar and nonpolar wood tar samples, Teflon filter loaded samples were extracted using a mixture of tetrahydrofuran and dichloromethane (1:1, *v/v*), the extracts were then concentrated using a mild N_2 flush and coated onto polished KBr windows uniformly (Diameter: 13 mm, Thickness: 2 mm, Spectra-Tech Inc.). The coated windows were further dried in N_2 purge before being analyzed. To the polar wood tar aerosol, particles were directly impacted onto KBr window. IR spectra for the samples were recorded over the range of 4000-400 cm^{-1} at room temperature using 32 scans at 2 cm^{-1} resolution. Ultrapure N_2 flush in the FT-IR cabinet was applied during spectra recording to avoid environmental CO_2 and moisture influence. The spectrum baseline was determined by analyzing the blank KBr window and subtracted the blank from the sample spectrum.

S5.4. GC×GC/EI-HR-ToF-MS. Solvent extracts were prepared by washing each operational blank and sampled Teflon filters in methanol using vortex shaking (Vortex Genie-2, Scientific Industries) method, the extracts were treated with filtration (0.2 μm PTFE syringe filter, Pall Life Science) and concentrated via gentle N_2 blowing, ensuring high extraction efficiency, clarity, and high concentrations of the extracts. Afterward, portions of the extracts were analyzed by a two-dimensional gas chromatography coupled to electron impact ionization high-resolution multi-reflection time-of-flight mass spectrometry (GC×GC/EI-HR-ToF-MS) to reveal their molecular composition. The description and operation of this instrument can be found elsewhere.[15,16] In brief, the comprehensive GC×GC is performed with a first dimension medium-polarity capillary column (59 m×0.25 mm i.d.×0.1 μm, BPX50, SGE Analytical Science, Ringwood, Australia) and a nonpolar second dimension column (2.4 m×0.10 mm i.d.×0.1 μm, BPX1, SGE Analytical Science, Ringwood, Australia) to separate organic compounds by their diverse volatility and polarity. After sample injection via programmable temperature vaporization (50-400°C at 1 °C s^{-1}), the GC oven was ramped from initial 50 ºC (5 min hold) to 310 ºC at 2 ºC min^{-1} and held for 5 min. A dual-stage thermal modulator, consisting of a guard nonpolar column (0.1 m×0.10 mm i.d.×0.1 μm, BPX1, SGE Analytical Science, Ringwood, Australia), was used as the interface between the two columns, where the effluent from the first column was cryogenically focused and periodically heated for rapid transfer into the second column with modulation period of 5.0 s. The second column was housed in a secondary oven, which was maintained at 5 ºC above the main oven temperature during temperature-rise period. Analytes were ionized via electron impact ionization (70 eV) and spectra were collected with a high-resolution ($m/\Delta m$>25,000) multi-reflection time-of-flight mass spectrometer.

S5.5. (-)ESI-Q-ToF-MS. Electrospray ionization (ESI) coupled with a quadrupole time-of-flight tandem mass spectrometry (Xevo G2 Q-ToF MS, Waters, Manchester, UK) provided detailed molecular characterization of organic compounds due to its high resolution ($m/\Delta m \geq 30{,}000$) and mass accuracy (≤5 ppm). ESI is commonly used soft ionization method that minimizes fragmentation of analytes, allowing for detection of intact molecules. These analytical approaches were applied to characterize the complex mixture of wood tar materials before and after NO_3 radical oxidation. After optimization, the extracts were directly infused at a flow rate of 10 μL min^{-1} and monitored in negative ESI mode. All spectra were acquired in the mass range 50–2000 m/z. These analyses were performed using a capillary voltage of 2.50kV, a source temperature of 120°C, a cone voltage of 20V. The desolvation temperature was set to 250°C and the desolvation gas (N_2) flow rate was approximately 6 L min^{-1}. All measurements were done with Leucine-Enkephalin (200 μg μL^{-1}) as

a lockspray reference at flow rate of 10 μL min^{-1} to ensure mass accuracy and follow resolution mode. Data acquisition and recording were done by Waters MassLynx v4.2 software. The ESI-HRMS data were processed with an open source software toolbox, MZmine 2 (http://mzmine. github.io/), to perform signal deconvolution and peak assignment. Peaks with signal to noise ratio less than 10 and peaks appeared in blanks were discarded. Formula assignments were performed using following constraints for the number of atoms in the ions: 2≤ C ≤100, 2≤ H ≤200, N≤3, O ≤50, S ≤1, and Cl ≤1 within 0.001 Δm/z tolerance or accuracy ≤ 5 ppm. Moreover, some other constraints include double-bond equivalent (DBE) to carbon ratio (DBE/C ≤ 1), elemental ratios (0.4≤ H/C ≤2.2, O/C ≤1.2, N/C ≤0.5, S/C ≤0.2), and carbon oxidation state ($\overline{OS}$, -3.5≤$\overline{OS}$ ≤3.5) were applied.

For an individual compound, DBE and $\overline{OS}$ of $C_cH_hO_oN_n$ can be calculated as follows[17,18]:

$$DBE = 1 + \frac{n-h}{2} + c \qquad \text{S 1 3}$$

$$\overline{OS} = 2 \times \frac{o}{c} - \frac{h}{c} - 5 \times \frac{n}{c} \qquad \text{S 1 4}$$

Where c, h. o, and n are the atom number for C, H, O, and N, respectively. Both DBE and $\overline{OS}$ do not consider S condition to the chemical formula, and DBE assumes a valence of 3 for nitrogen, therefore, Equation S13 may underestimate the real DBE for nitro-compounds (R-NO_2) and organonitrate (R-ONO_2).

In view of the molecular complexity in bulk materials like wood tar aerosol, hundreds and thousands of compounds may be identified from mass spectrum, it is common to express the bulk composition as averaged elemental composition and characteristics (C, H, O, N, S, O/C, H/C, N/C, DBE, and $\overline{OS}$) via Equation S15[19]:

$$\langle Y \rangle = \frac{\sum_i x_i Y_i}{\sum_i x_i} \qquad \text{S 1 5}$$

Where Y_i is elemental composition and ratios for i_{th} molecular formula, x_i is intensity or peak height of the assigned i_{th} molecular formula.

S5.6. HPLC-PDA-(-)ESI/HRMS analysis. Unprocessed and NO_3-reacted wood tar aerosol extracts were also analyzed using a Vanquish ultra-high performance liquid chromatographic (HPLC) system coupled with a photodiode array detector (PDA) and an Q Exactive HF-X high resolution mass spectrometer (HRMS) equipped with an electrospray ionization (ESI) source (all HPLC-PDA-ESI/HRMS modules are from Thermo Scientific, Inc). Samples were separated on a reversed-phase column (Luna C18, 150×2 mm^2, 5 μm particles, 100 Å pores, Phenomenex, Inc.) using a binary solvent mixture containing LC-MS grade water with 0.1% (v/v) formic acid (A) and LC-MS grade acetonitrile with 0.1% (v/v) formic acid (B). A flow rate of 200 μL min^{-1} and a sample injection volume of 5 μL were used. The analyte was separated using a stepwise gradient; 0-3 min at 90% of A, 3-90 min a linear gradient to 0% of A, 90-100 min held at 0% of A, 100-101 min a linear gradient to 90% of A, and 101-120 min held at 90% of A to re-equilibrate the column at the initial mobile phase conditions for the next sample. UV-Vis absorption spectra for the eluted chemicals were measured using the PDA detector over the wavelength range of 200-700 nm. We specifically focused on negative mode ESI due to its preference in detecting compounds with acidic protons (e.g., nitro-phenols and carboxylic acids).[20,21] The raw data were acquired using Xcalibur software (Thermo Scientific) and were processed using Xcalibur software and an online LC-MS data processing software (MZmine-2.38). Formula assignment was performed according to the Xcalibur and MIDAS formula calculator. ESI-HRMS in combination with high-performance liquid chromatography (HPLC) with a photodiode array (PDA) detector was used to separate BrC compounds based on their retention times in conjunction with their light-absorbing properties, thus elucidating their plausible molecular structures. Details refer to the previous work.[20,21]

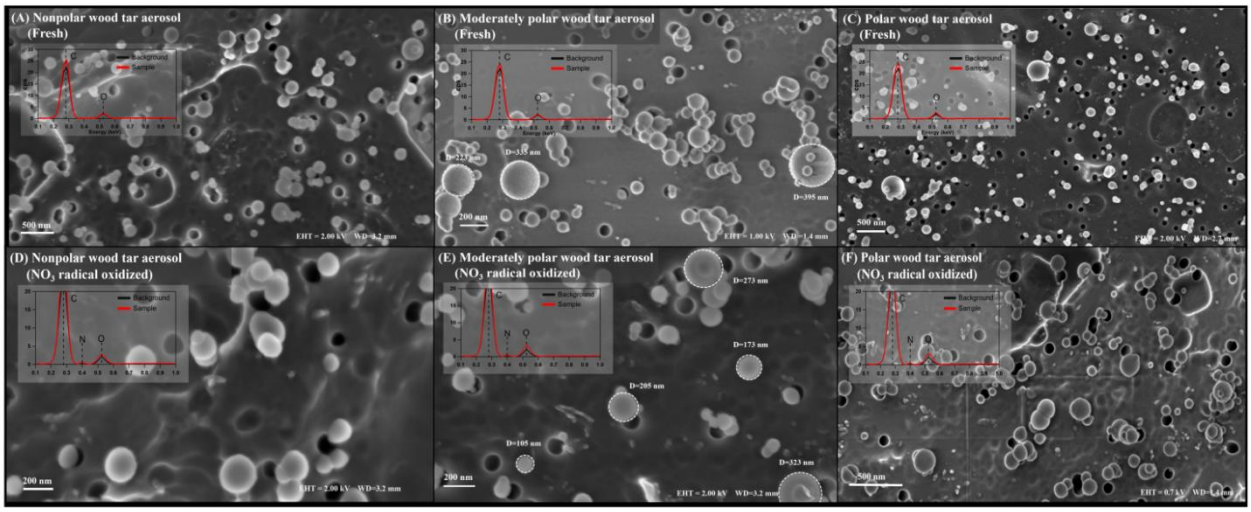

Figure S1. Individual particle morphology and elemental compositions for (A)-(C) fresh, and (D)-(F) after 13.3 h equivalent ambient NO_3 radical exposure processed wood tar aerosols. EDX (X-ray energy-disperse spectrometer) spectra averaged from selected particles are shown to indicate the semi-quantitative elemental composition. Wood tar aerosols generated in the laboratory are spherical amorphous carbonaceous particles containing major C and minor O, after exposing to NO_3 radicals, weak nitrogen additions were detected. The nitrogen signals are probably underestimated due to evaporation or/and decomposition of the nitrogen-bearing organic products in EDX measurements. Semi-quantitative elemental ratios of O/C were calculated as 0.058, 0.108, and 0.345 for fresh nonpolar, moderately polar, and polar wood tar particles, respectively. After NO_3 radical process, the ratios increased to 0.066, 0.229, 0.478 in accordance with the polarity.

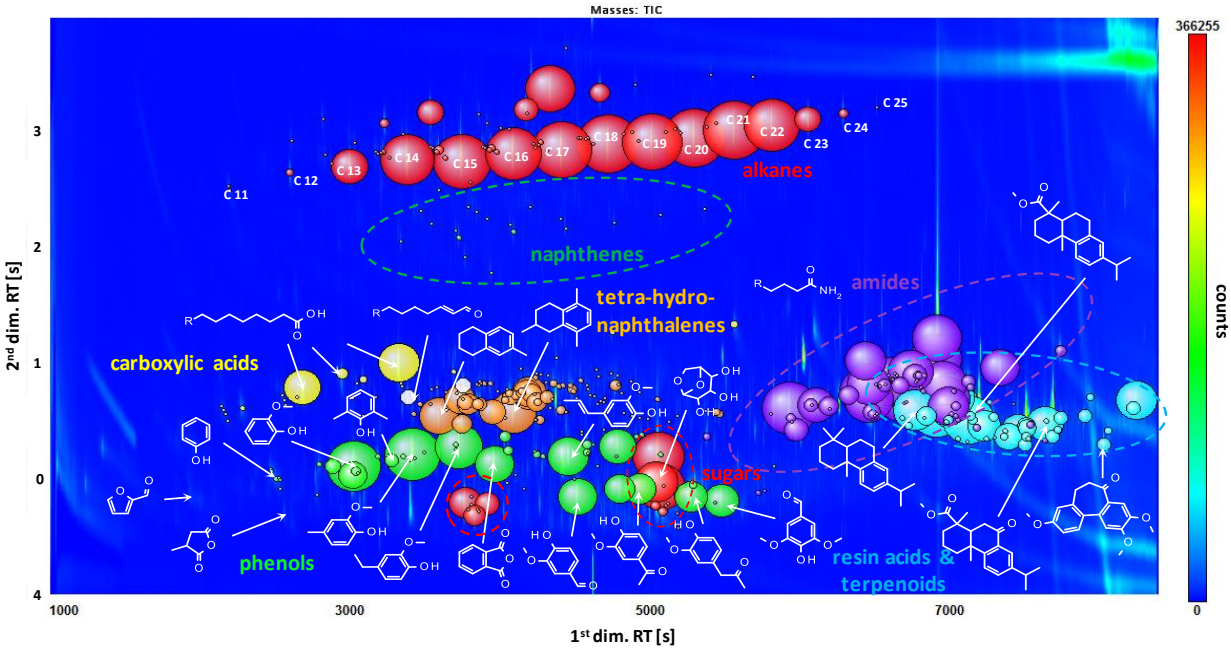

Figure S2. GC×GC/EI-HR-ToF-MS chromatogram of fresh moderately polar wood tar aerosol. Second dimension retention time (RT) is shifted 4 seconds to adjust for wrap around. Exemplary chemical structures of most abundant peaks are shown for identified chemical groups (e.g., phenols, sugars, carboxylic acids, amides, naphthalenes, naphthenes, amides, etc). The circle size indicates relative signal intensity.

Table S1. Summarized optical and density results for fresh and NO_3 oxidized wood tar aerosols

Wood tar aerosol	CRDS-PAS @ 404 nm	SSA @ 404 nm	BBCES @ 404 nm	-ln(*k*)/ln(*λ*)	AAE	Particle density (g cm^{-3})
Polar wood tar_fresh	(1.536 ± 0.020) + (0.007 ± 0.001)i	0.968	(1.545 ± 0.007) + (0.008 ± 0.003)i	8.103	9.103	1.350 ± 0.015
8.26 ± 2.33 h EAN	(1.533 ± 0.011) + (0.009 ± 0.003)i	0.956	(1.538 ± 0.007) + (0.009 ± 0.003)i	7.863	8.863	1.341 ± 0.014
11.66 ± 2.74 h EAN	(1.524 ± 0.005) + (0.013 ± 0.001)i	0.942	(1.522 ± 0.010) + (0.018 ± 0.006)i	4.739	5.739	1.332 ± 0.016
13.26 ± 3.09 h EAN	(1.520 ± 0.009) + (0.014 ± 0.003)i	0.936	(1.506 ± 0.013) + (0.023 ± 0.005)i	4.103	5.103	1.319 ± 0.015
Moderately polar wood tar_fresh	(1.589 ± 0.004) + (0.018 ± 0.002)i	0.931	(1.584 ± 0.005) + (0.016 ± 0.001)i	8.444	9.444	1.248 ± 0.012
8.26 ± 2.33 h EAN	(1.579 ± 0.002) + (0.022 ± 0.001)i	0.917	(1.570 ± 0.003) + (0.021 ± 0.001)i	6.727	7.727	1.244 ± 0.014
11.66 ± 2.74 h EAN	(1.574 ± 0.003) + (0.024 ± 0.002)i	0.907	(1.553 ± 0.003) + (0.022 ± 0.001)i	5.580	6.580	1.223 ± 0.011
13.26 ± 3.09 h EAN	(1.561 ± 0.006) + (0.028 ± 0.002)i	0.891	(1.534 ± 0.002) + (0.031 ± 0.001)i	4.739	5.739	1.193 ± 0.007
Nonpolar wood tar_fresh	(1.597 ± 0.004) + (0.024 ± 0.001)i	0.915	(1.608 ± 0.002) + (0.023 ± 0.002)i	6.753	7.753	1.194 ± 0.006
8.26 ± 2.33 h EAN	(1.585 ± 0.003) + (0.027 ± 0.003)i	0.901	(1.593 ± 0.003) + (0.026 ± 0.002)i	5.701	6.701	1.182 ± 0.009
11.66 ± 2.74 h EAN	(1.582 ± 0.004) + (0.029 ± 0.002)i	0.892	(1.585 ± 0.004) + (0.032 ± 0.002)i	5.418	6.418	1.182 ± 0.008
13.26 ± 3.09 h EAN	(1.576 ± 0.005) + (0.032 ± 0.003)i	0.884	(1.567 ± 0.005) + (0.036 ± 0.003)i	5.121	6.121	1.181 ± 0.004

Note: CRDS-PAS retrieved RI contains real part from CRDS measurement and imaginary part from PAS measurement. SSA for 250 nm wood tar aerosol was calculated using extinction and absorption cross section values from CRDS-PAS directly measurement at 404 nm. Imaginary *k*-derived absorption Angström Exponent (AAE) was regressed over wavelength range of 315-450 nm. For polar wood tar aerosol, AAE was fitted over the measured effective wavelength range of 315-425 nm

S6. Chemical Box Model Simulations.

S6.1. NO_3 radical and N_2O_5 aerosol loss in the AFR. Heterogeneous reactions occurred when wood tar particles mixed with gaseous N_2O_5 and NO_3 radicals in the AFR. However, the conversion efficiency of N_2O_5 to NO_3 at equilibrium depends on the precursor concentration and temperature. At room temperature and initial N_2O_5 concentration of 500-1000 ppbv, less than 10% of N_2O_5 will thermally dissociate to produce NO_3 radicals at equilibrium. N_2O_5 and NO_3 radicals involve different heterogeneous reaction pathways. Through hydrolysis to produce nitric acid is the main reaction of N_2O_5 on particle surfaces, previous studies confirmed that N_2O_5 taken by organic surface can be efficient nitrating agent.[22,23] In parallel, NO_3 radicals can initiate a series of oxidation reactions in the presence of NO_2 and O_2.[24-26] The overall sink of NO_3 radical and N_2O_5 in the experiment can be simply described by the pseudo-first-order loss to the particle surface and to the wall of the AFR via Equation S16-S18:[27,28]

$$\frac{d[G]}{dt} = -(k_p[G] + k_w[G]) \qquad \text{S16}$$

$$k_p = \frac{\gamma_{eff} \times \omega \times S}{4} = \frac{1}{4}\omega \times S \times (\frac{1}{\gamma_p} + \frac{1}{\Gamma_{diff-p}})^{-1} \qquad \text{S17}$$

$$k_w = \frac{\gamma_{eff} \times \omega}{4} \times \frac{S_{AFR}}{V_{AFR}} = \frac{\omega}{D_{\text{int}}} \times (\frac{1}{\gamma_w} + \frac{1}{\Gamma_{diff-w}})^{-1} \qquad \text{S18}$$

Where k_p and k_w represent pseudo-first order loss rate to particle surface and to reactor inner wall, respectively. γ_{eff} is effective uptake coefficient (unitless) for gas G. ω is molecular speed of gas G (ω, m s^{-1}). S is total particle surface area exposed to reactant (cm^2 m^{-3}). S_{AFR} and V_{AFR} are inner surface area and volume of the reactor. D_{int} is the inner diameter of the cylindrical flow reactor we used. γ_p and γ_w are uptake coefficient (unitless) to particle surface and to the AFR inner wall. Γ_{diff} describes the gas phase diffusion limitation (unitless) in particle and reactor surface uptake. For the uptake onto monodisperse spherical particles, several methods have been suggested to calculate $\Gamma_{diff\text{-}p}$.[29,30] The regular method is described as the Fuchs-Sutugin equation in S19:

$$\frac{1}{\Gamma_{diff-p}} = \frac{0.75 + 0.286 \times \text{K}n}{\text{K}n \times (\text{K}n + 1)} \qquad \text{S19}$$

Where K_n is Knudsen number, given by Equation S20:

$$\text{K}n = \frac{6D}{\omega \times Dp} \qquad \text{S20}$$

The Knudsen number is a function of particle diameter (Dp, nm), gas-phase diffusion coefficient (D, torr cm^2 s^{-1}) for gaseous molecular G, and molecular speed ω. For fast uptake process (lower Γ_{diff} and higher γ) and large particles, gas phase diffusion can limit the overall rate of the uptake of G onto the particle surface. For heterogeneous reactions occurring with polydispersed particles, we can rewrite the above first-order reaction kinetic k_{het} as Equation S21, taking first-order wall loss of the particles into account:

$$k_p = \frac{1}{4}\omega \times \sum_i \left[N_i \times \pi \times D_i^2 \times (1 - k_{wall-p}t) \times (\frac{1}{\gamma_p} + \frac{1}{\Gamma_{diff-p}})^{-1} \right] \qquad \text{S21}$$

Where Ni is number concentration (m^{-3}) for particle of size Di (nm), $k_{wall\text{-}p}$ is first-order wall loss rate (s^{-1}) for particles.

In our experiments, we did not observe significant wood tar particle losses to the wall of the AFR based on SMPS and CPC measurements. Thereby, the wall loss rate for wood tar particles can be neglected to get Equation S22:

$$k_p = \frac{1}{4}\omega \times \sum_i \left[N_i \times \pi \times D_i^2 \times (\frac{1}{\gamma_p} + \frac{1}{\Gamma_{diff-p}})^{-1} \right] \qquad \text{S22}$$

$\Gamma_{diff\text{-}w}$ is the NO_3 radical and N_2O_5 wall loss to the AFR, as suggested as Equation S23:

$$\frac{1}{\Gamma_{diff-w}} = \frac{\omega \times D_{\text{int}}}{4 \times 3.66 \times D} \qquad \text{S 2 3}$$

For the case where the loss rate of gases to the reactor wall is not determined by surface reactivity, but by the diffusion through the gas phase ($\gamma_w > \Gamma_{wall} \sim 7\times10^{-6}$), the following expression holds:

$$k_w = \frac{\omega}{D_{\text{int}}} \times (\frac{1}{\gamma_w} + \frac{1}{\Gamma_{diff\ w}})^{-1} \approx \frac{\omega \times \Gamma_{diff\ w}}{D_{\text{int}}} = \frac{4 \times 3.66 \times D}{D_{\text{int}}^{\ 2}} \qquad \text{S 2 4}$$

Equation S24 is valid for Peclet numbers in excess of ~20.[31] This study results in Peclet numbers ($Pe=D_{int}\times v/D$, where v is the average linear velocity of the gas flow) of ~26 for NO_3 radical and ~37 for N_2O_5.

The reactive uptake coefficient (γ) depends on the reactant and particle surface available.[32,33] Various values have been reported for NO_3 radicals and N_2O_5 uptake by different chemical surfaces. For NO_3 radical, the uptake coefficients vary considerably from approximately 2×10^{-4} for NO_3 on solid saturated organics up to $\gamma \geq 0.1$ for some liquid unsaturated organics and phenols.[34,35] Only a few values for biomass burning-related surrogates (e.g., hydrocarbon PAHs, phenols, levoglucosan, etc.) were reported to be in the range of 0.08-0.79 or 0.01-0.03 for NO_3 radicals and less than 6.6×10^{-5} for N_2O_5 at room temperature and pressure in dry air.[22,23,36] The reported reactive uptake coefficient of NO_3 radicals on methoxy-phenol surface can be ~3 orders of magnitude greater than those of NO_2 and N_2O_5.[32,35] From our previous work and HR-ToF-AMS/FT-IR results in this study, the wood tar aerosols we generated comprise large fractions of aromatics and phenols, then the uptake coefficient of 10^{-2} and 10^{-5} was applied for NO_3 radical and N_2O_5, respectively. According to Tang et al., averaged gas-phase diffusion coefficient of NO_3 is 92±46 torr cm^2 s^{-1}, and N_2O_5 has a diffusion coefficient of 65±33 torr cm^2 s^{-1}.[37] Based on number size distributions of wood tar aerosols measure from SMPS (Figure S3), the integrated heterogeneous reaction kinetics at environment condition (1 atm and 296.6 K) were calculated and together with wall loss rates were listed in Table S2:

Table S2. Estimated reaction kinetics for NO_3 radicals and N_2O_5 interaction with wood tar aerosols and reactor inner surface wall

Gas/ Wood tar aerosol	Pseudo-first-order reaction kinetics (k_p, s^{-1})				Pseudo-first-order wall loss rate (k_w, s^{-1})
	Nonpolar	Moderately polar	Polar	Average	
NO_3	$(1.73\pm0.21)\times10^{-2}$	$(1.88\pm0.13)\times10^{-2}$	$(1.85\pm0.15)\times10^{-2}$	$(1.82\pm0.21)\times10^{-2}$	0.031±0.015
N_2O_5	$(1.31\pm0.16)\times10^{-5}$	$(1.42\pm0.11)\times10^{-5}$	$(1.39\pm0.11)\times10^{-5}$	$(1.37\pm0.15)\times10^{-5}$	0.022±0.011

Sufficient denuders were used to remove solvents (H_2O, CH_3OH, CH_3CN) from atomized aerosols. Attention should still be paid to the residual gaseous solvents and their competitive reactions with N_2O_5 and NO_3 radicals in the AFR, due to their high vapor pressure and incomplete filtration through the denuders. The humidity downstream of the AFR in the polar tar aerosol experiment was less than 0.2% (upper limit H_2O molecule concentration of 1.536×10^{15} molecules cm^{-3} in the AFR). We assumed that the solvents were saturated in the gas phase from the atomizer (296.6±0.5 K, 1 atm) and each denuder has 80% filtration efficiency to remove gaseous solvent. The final gaseous CH_3CN and CH_3OH entering the flow tube reactor were estimated to be 7.830×10^{15} and 1.211×10^{16} molecules cm^{-3} at maximum, respectively.

A simplified model including 10 homogeneous reactions in the gas phase, 4 heterogeneous uptake reactions, and first-order wall loss of N_2O_5-NO_3-NO_2 was developed to estimate the reactive uptake of NO_3 radical and N_2O_5 by wood tar aerosol in the AFR.[32-38] The

kinetics and reaction pathways applied in model simulation were summarized in Table S3.

Table S3. Reaction pathways and rate constants for the modeling of the experiment

Reaction pathways		Reaction rate constant (295K) ($molec^{-1}$ cm^3 s^{-1})	Reactive uptake coefficient (γ)	First-order wall loss rate/ heterogeneous reaction kinetics (k_{het}, s^{-1})	Reference or source
Gaseous	$NO_3 + NO_2 \rightleftharpoons N_2O_5$	$k_{eq(T)} = 2.7\times10^{-27}\times e^{11000/T}$			Ayres et al., 2015
Gaseous	$NO_3 + NO_2 \rightarrow N_2O_5$	1.66×10^{-12}			NIST Kinetic
Gaseous	$N_2O_5 + H_2O \rightarrow 2HNO_3$	2.5×10^{-22}			NIST Kinetic
Gaseous	$NO_3 + H_2O \rightarrow HNO_3 + OH$	2.5×10^{-22}			NIST Kinetic
Gaseous	$NO_2 + NO_3 \rightarrow O_2 + NO + NO_2$	6.56×10^{-16}			NIST Kinetic
Gaseous	$NO_3 + NO_3 \rightarrow O_2 + 2NO_2$	2.29×10^{-16}			NIST Kinetic
Gaseous	$CH_3CN + NO_3 \rightarrow CH_3CN\text{-}NO_3$	$<5.0\times10^{-19}$			NIST Kinetic
Gaseous	$CH_3CN + N_2O_5 \rightarrow CH_3CN\text{-}N_2O_5$	$<6.0\times10^{-23}$			NIST Kinetic
Gaseous	$CH_3OH + NO_3 \rightarrow CH_3OH\text{-}NO_3$	1.3×10^{-18}			NIST Kinetic
Gaseous	$CH_3OH + N_2O_5 \rightarrow CH_3OH\text{-}N_2O_5$	$<2.0^{-19}$			NIST Kinetic
Particulate	$NO_3 \rightarrow P_{(Ar)}\text{-}NO_3$		0.08-0.79, $(1.3\text{-}26.1)\times10^{-3}$, 0.28-0.22	$(1.82\pm0.21)\times10^{-2}$	Gross, S et al., 2008; 2009; Knopf et al., 2011
Particulate	$N_2O_5 \rightarrow P_{(Ar)}\text{-}N_2O_5$		$\leq6.6\times10^{-5}$ [a], $(3.7\text{-}5.8)\times10^{-5}$ [b]	$(1.37\pm0.15)\times10^{-5}$	Gross, S et al., 2008; 2009; Knopf et al., 2011
Particulate	$NO_2 \rightarrow P_{(Ar)}\text{-}NO_2$		4.3×10^{-9}, $\leq8.5\times10^{-6}$	$\sim1.42\times10^{-8}$	Li et al., 2010; Gross, S et al., 2008
Particulate	$HNO_3 \rightarrow P_{(Ar)}\text{-}HNO_3$		$\leq2.5\times10^{-5}$	$\sim7.07\times10^{-5}$	Gross, S et al., 2008
Wall loss	$NO_3 \rightarrow$ wall			0.031±0.015	This study
Wall loss	$N_2O_5 \rightarrow$ wall			0.022±0.011	This study

Note: Only first-step reactions were considered, $CH_3CN\text{-}NO_3$ and $CH_3OH\text{-}NO_3$ simply indicate the class of NO_3 reaction products with gaseous acetonitrile and methanol. $P_{(Ar)}$ represent aromatic-specific particles. NIST kinetics can be sourced: https://kinetics.nist.gov/kinetics/index.jsp

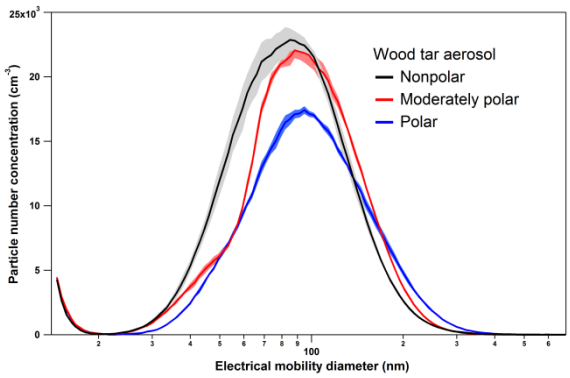

Figure S3. Size distribution for initial nonpolar, moderately polar, and polar wood tar aerosols in the aerosol flow tube reactor

A complex pathway simulator (COPASI, http://copasi.org/) was used to perform the simulation. The box-model time traces of molecular concentrations for N_2O_5, NO_3 radical, wood tar aerosol surface uptake of NO_3 and N_2O_5 are displayed in Figure S4. It is noteworthy that the rapid conversion of N_2O_5 and surface uptake of NO_3 and N_2O_5 within their retention time (165s) occurred in the AFR, and surface uptake of NO_3 radicals by wood tar aerosols exceeds by one or two orders of magnitudes compared to the uptake of N_2O_5. We therefore concluded that NO_3 radical reactions should be the dominant pathway to oxidize wood tar aerosols, though N_2O_5 can also be nitrating agent at dehydrated organic surface.

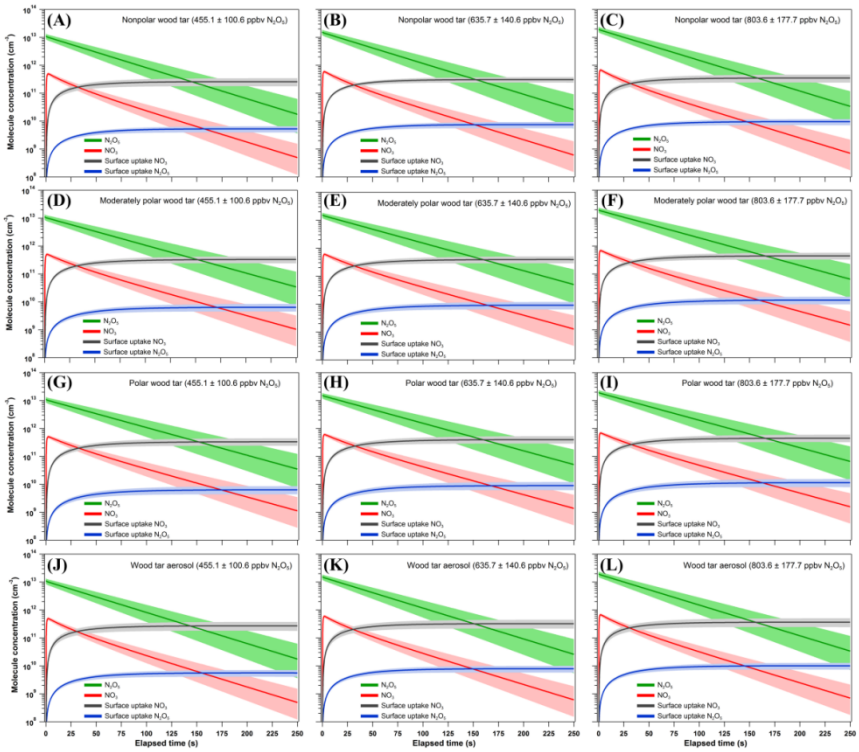

Figure S4. Box model time traces of molecular concentrations for N_2O_5, NO_3 radical, and surface uptake of NO_3 and N_2O_5 as a function of wood tar particle polarity and initial N_2O_5 concentration. (A)-(C) nonpolar wood tar aerosol, (D)-(F) moderately polar wood tar aerosol, (G)-(I) polar wood tar aerosol, (J)-(L) average result for wood tar aerosol as a function of initial N_2O_5 concentration in the range of 455-804 ppbv.

S6.2. Quantification of nighttime smoke particle NO_3 aging. The NO_3 mixing ratios measured *in situ* in urban and rural areas have a large variance, and at ground level in cities and suburban areas next to power plants, the NO_3 concentration may be below the detection limits (0.5-10 pptv) of most instruments due to the high mixing ratio of NO and or severe particle pollution. At rural areas and forest environments or away from urban areas, NO_3 mixing ratios can reach up to several hundred pptv and N_2O_5 up to a few ppbv.[6,39,40] Though in polluted environments, such as regions influenced by a fire, where NO_3 radical and N_2O_5 have an ultra-low steady-state concentration, the reaction between O_3 and NO_2 in high concentrations can maintain a rapid formation rate for NO_3 radicals, which can be up to several ppbv hr^{-1}.[41,42] Moreover, the gaseous pollutants from biomass burning can act as a major NO_3 radical sink at nighttime and less than 1% of NO_3/N_2O_5 loss is due to uptake by the smoke aerosol.[41]

To compare with field smoke particle aging due to NO_3 and N_2O_5 reactions, the NO_3/N_2O_5 chemistry in the aerosol flow tube was

quantified as equivalent ambient nighttime NO_3/N_2O_5 reactions (*EAN*). We estimated the uptake of NO_3 and N_2O_5 by wood tar particle downstream of the AFR (RT~165) via the above chemical box model simulation. The uptake of the two species were then normalized to wood tar particle surface area density via:

$$P_{NO_3} = \frac{[NO_3]_{upt} + [N_2O_5]_{upt}}{S} \quad \text{S 2 5}$$

Where $[NO_3]_{upt}$ and $[N_2O_5]_{upt}$ are surface uptake of NO_3 and N_2O_5 from Figure S4, respectively. S is the wood tar particle surface area density, P_{NO3} is the normalized surface uptake of NO_3 and N_2O_5 as bulk.

According to Decker et al. and Steven S.B. et al.,[41,42] a simple equilibrium between ambient NO_3 radical sink and source in fire plumes within the residual layer can be built with assumption of a steady state for both NO_3 and N_2O_5:

$$k_{NO_2-O_3}[NO_2][O_3] \approx \sum_i k_{NO_3-VOCi}[VOC_i][NO_3] + k_{NO_3}^{aerosol}[NO_3] \quad \text{S 2 6}$$

$$k_{NO_3}^{aerosol} = K_{eq}[NO_2]k_{N_2O_5-aerosol} + k_{NO_3-aerosol} \quad \text{S 2 7}$$

Where the left part of Equation S26 is NO_3 radical production rate from reaction of NO_2 and O_3, the right side is instant NO_3 radical consumption via homogeneous reactions with VOCs and smoke particle surface uptake. Equation S27 depicts NO_3 radical and N_2O_5 uptake to particle surface. The estimated NO_3 radical reactivity due to homogeneous biomass burning VOCs reaction is a factor of 100-1000 greater than smoke aerosol surface uptake in fresh emissions.[41] Considering the rapid aging, dilution, and smoke particle growth due to condensation and coagulation during biomass burning emissions transport, the NO_3 radical reactivity due to surface uptake should weigh more in the total reactivity. Here we assumed a median and constant ratio of 500 for total NO_3 reactivity to smoke particle uptake during nighttime atmospheric process:

$$\sum_i k_{NO3-VOCi}[VOC_i] + k_{NO_3}^{aerosol} \approx 500 \times k_{NO_3}^{aerosol} \quad \text{S 2 8}$$

Normalize the NO_3 radical uptake rate to smoke particle surface area:

$$R_{NO_3}^{aerosol} = \frac{k_{NO_3}^{aerosol}[NO_3]}{S_{aerosol}} \approx \frac{k_{NO_2-O_3}[NO_2][O_3]}{500 \times S_{aerosol}} \quad \text{S 2 9}$$

Where $R_{NO_3}^{aerosol}$ is the smoke particle surface area normalized NO_3 radical uptake rate, $S_{aerosol}$ is surface area density for ambient smoke aerosol. Then the AFR reaction between NO_3-N_2O_5 and wood tar particles can be quantified to practical aging time for field fire emissions at nighttime, termed as "equivalent ambient nighttime NO_3/N_2O_5 reaction (EAN)" combining Equation S25 and S29:

$$EAN = \frac{P_{NO_3}}{R_{NO_3}^{aerosol}} = \frac{P_{NO_3} \times 500 \times S_{aerosol}}{k_{NO_2-O_3}[NO_2][O_3]} \quad \text{S 3 0}$$

The ambient NO_2 and O_3 are commonly in the range of 10-50 ppbv in field fire influenced regions or next to the fire plumes, while smoke particles have practical concentrations with average $PM_{2.5}$ within 50 μg m^{-3} at nighttime.[41-43] In this study, typical ambient NO_2, O_3, and smoke particle surface density were taken as 25 ppbv, 35 ppbv, and 2×10^8 nm^2 cm^{-3}, respectively, referring to reference and also our previous work.[41-43] The estimated *EAN* under such condition were estimated for wood tar particles and presented in Table S4.

Table S4. Chemical-box model estimated equivalent ambient NO_3 radical aging time for wood tar particles

Initial N_2O_5 density (ppbv)	Wood tar aerosol (EAN: h)			
	Nonpolar	Moderately polar	Polar	Average
455.1 ± 100.6	7.52 ± 2.16	9.37 ± 3.19	8.64 ± 3.03	8.26 ± 2.33
635.7 ± 140.6	10.61 ± 2.57	13.42 ± 3.79	12.17 ± 3.60	11.66 ± 2.74
803.6 ± 177.7	12.05 ± 2.91	15.36 ± 4.28	13.87 ± 4.07	13.26 ± 3.09

Table S5. Summarized HR-ToF-AMS results for fresh and NO_3 oxidized wood tar aerosols

Wood tar aerosol	O:C	H:C	N:C	f_{NO3}	$f_{m/z>100}$
Polar wood tar_fresh	0.528 ± 0.006	1.773 ± 0.006	0.003 ± 0.002	0.4 wt.%	5.5 wt.%
8.26 ± 2.33 h *EAN*	0.614 ± 0.003	1.723 ± 0.005	0.030 ± 0.003	2.7 wt.%	4.3 wt.%
11.66 ± 2.74 h *EAN*	0.675 ± 0.009	1.719 ± 0.004	0.056 ± 0.004	4.6 wt.%	4.3 wt.%
13.26 ± 3.09 h *EAN*	0.716 ± 0.006	1.714 ± 0.006	0.084 ± 0.002	6.7 wt.%	4.2 wt.%
Moderately polar wood tar_fresh	0.312 ± 0.006	1.633 ± 0.006	0.002 ± 0.002	0.4 wt.%	25.2 wt.%
8.26 ± 2.33 h *EAN*	0.368 ± 0.012	1.614 ± 0.005	0.021 ± 0.001	2.2 wt.%	20.6 wt.%
11.66 ± 2.74 h *EAN*	0.433 ± 0.007	1.604 ± 0.008	0.047 ± 0.001	4.7 wt.%	18.3 wt.%
13.26 ± 3.09 h *EAN*	0.468 ± 0.010	1.600 ± 0.004	0.076 ± 0.002	7.2 wt.%	15.3 wt.%
Nonpolar wood tar_fresh	0.186 ± 0.005	1.568 ± 0.006	0.000 ± 0.000	0.1 wt.%	32.9 wt.%
8.26 ± 2.33 h *EAN*	0.273 ± 0.005	1.563 ± 0.007	0.026 ± 0.002	3.0 wt.%	26.7 wt.%
11.66 ± 2.74 h *EAN*	0.338 ± 0.004	1.533 ± 0.005	0.048 ± 0.004	5.1 wt.%	27.1 wt.%
13.26 ± 3.09 h *EAN*	0.389 ± 0.007	1.528 ± 0.008	0.094 ± 0.004	9.4 wt.%	24.6 wt.%

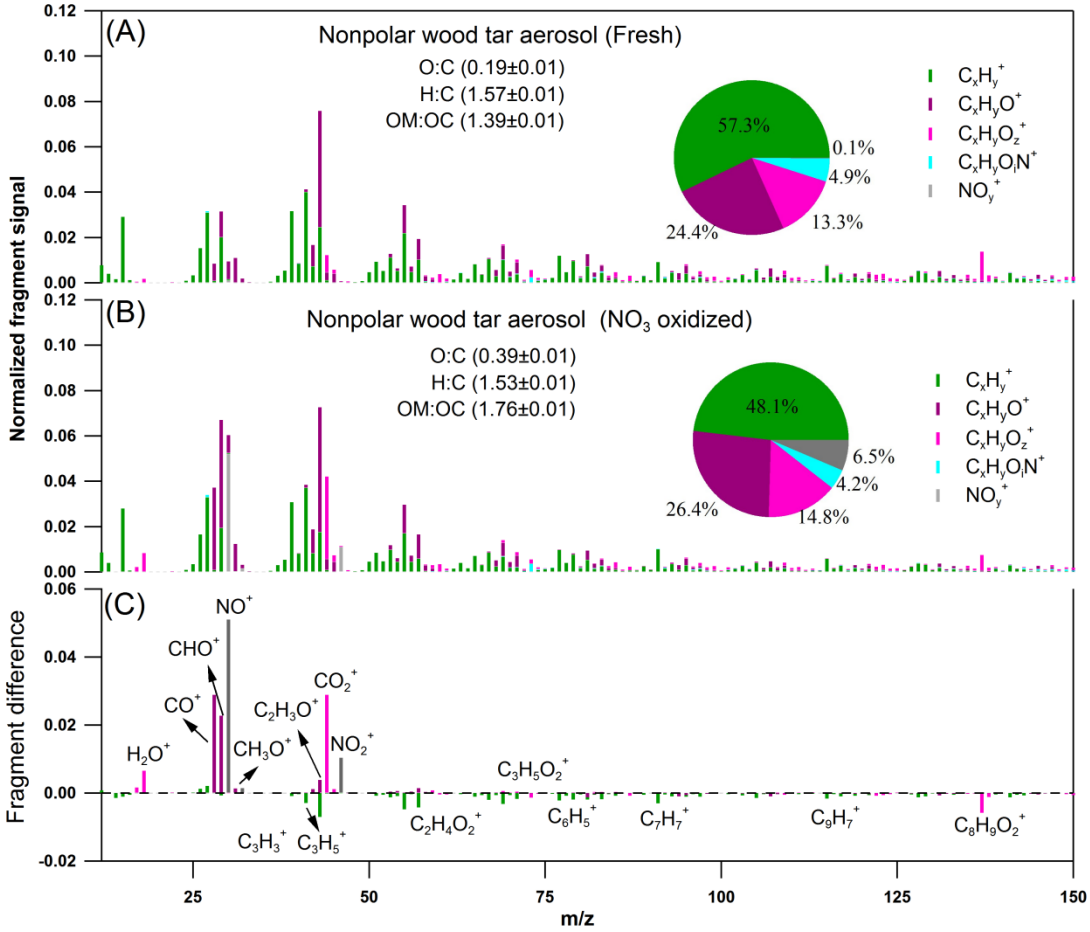

Figure S5. Comparison of AMS result for nonpolar wood tar aerosol before (A) and after 13.3 h equivalent ambient NO_3 radical oxidation (B). The mass spectra difference was presented in (C). Five groups were classified based on fragment elemental compositions, e.g., $C_xH_y^+$, $C_xH_yO^+$, $C_xH_yO_z^+$, $C_xH_yO_iN^+$, and NO_y^+, where x≥1, y≥1, z>1, i≥0. $H_xO_y^+$ fragments were grouped in $C_xH_yO_z^+$. Mass fractions of these five groups were shown as inserted pie-chart.

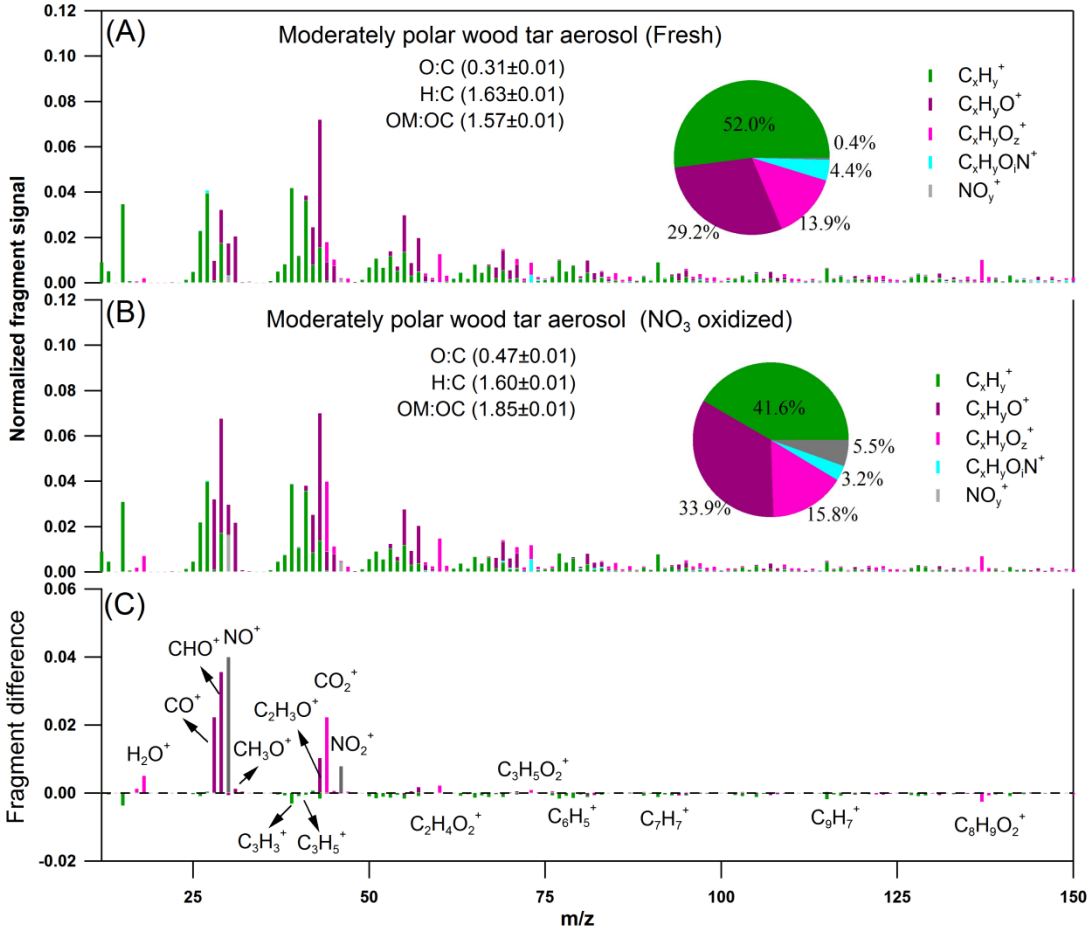

Figure S6. Comparison of AMS result for wood tar aerosol with moderate polarity before (A) and after 13.3 h equivalent ambient NO_3 radical oxidation (B). The mass spectra difference was presented in (C). Five groups were classified based on fragment elemental compositions, e.g., $C_xH_y^+$, $C_xH_yO^+$, $C_xH_yO_z^+$, $C_xH_yO_iN^+$, and NO_y^+, where x≥1, y≥1, z>1, i≥0. $H_xO_y^+$ fragments were grouped in $C_xH_yO_z^+$. Mass fractions of these five groups were shown as inserted pie-chart.

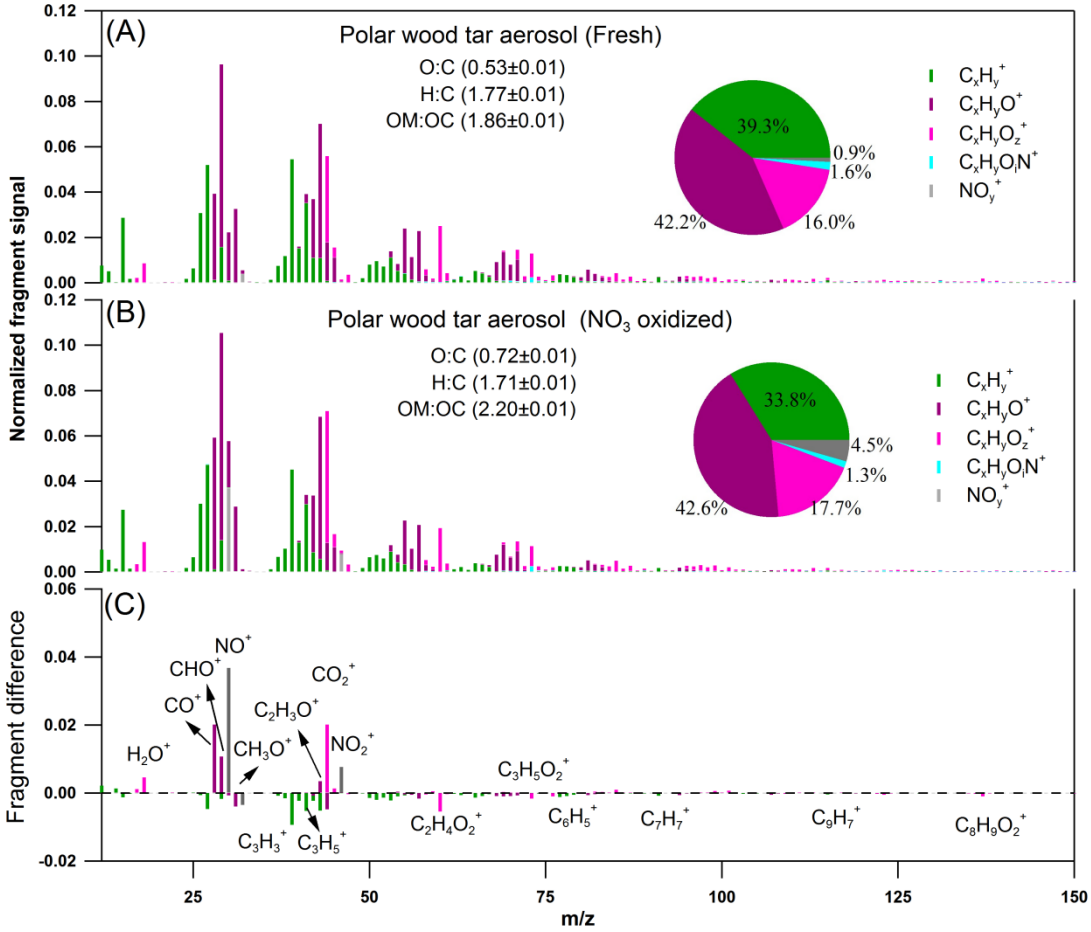

Figure S7. Comparison of AMS result for polar wood tar aerosol before (A) and after 13.3 h equivalent ambient NO_3 radical oxidation (B). The mass spectra difference was presented in (C). Five groups were classified based on fragment elemental compositions, e.g., $C_xH_y^+$, $C_xH_yO^+$, $C_xH_yO_z^+$, $C_xH_yO_iN^+$, and NO_y^+, where x≥1, y≥1, z>1, i≥0. $H_xO_y^+$ fragments were grouped in $C_xH_yO_z^+$. Mass fractions of these five groups were shown as inserted pie-chart.

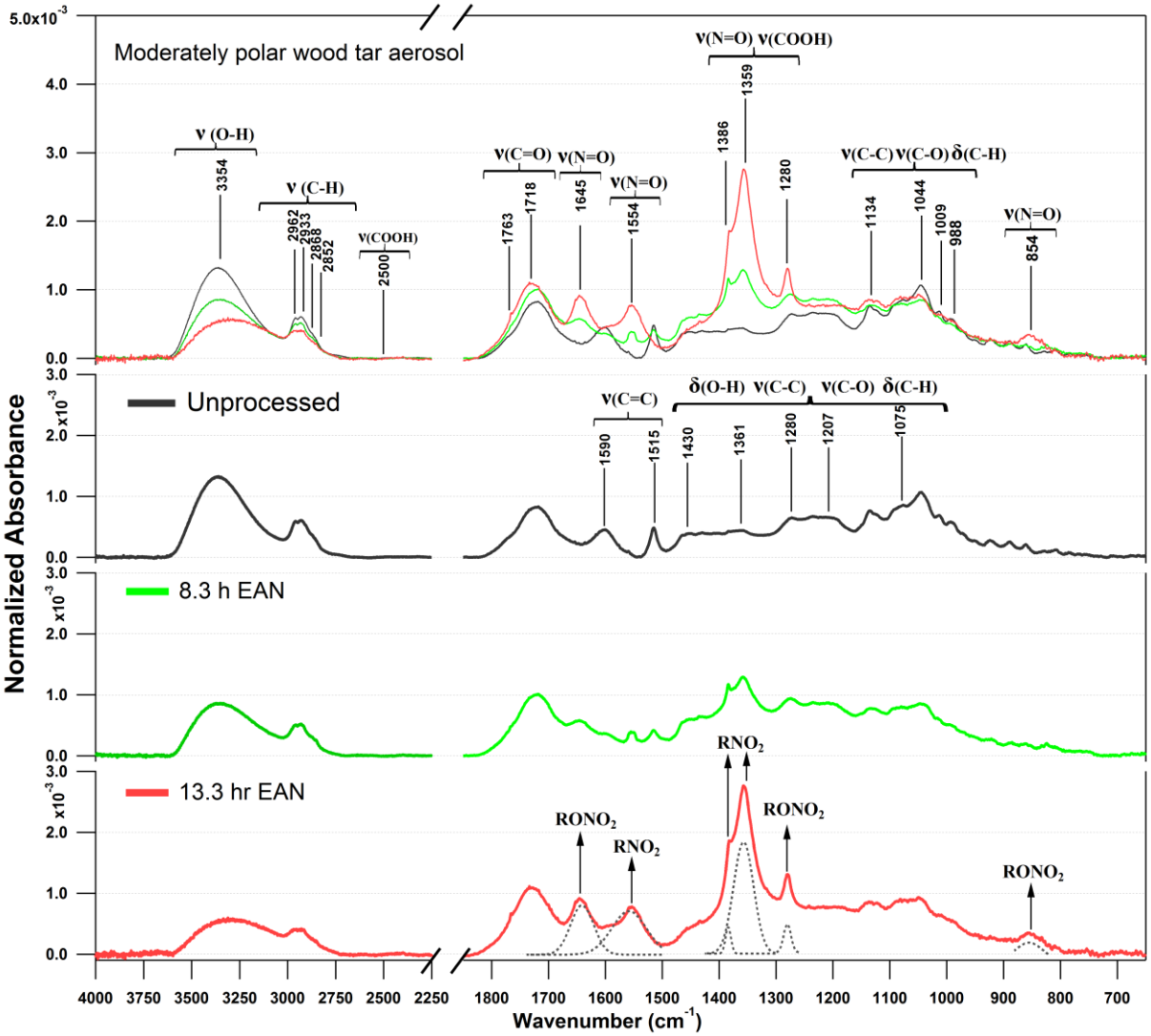

Figure S8. FT-IR spectra for moderately polar wood tar particles as a function of NO_3 radical exposure. The signal was normalized to the entire spectral area. Therefore, the formation of new functional groups can be directly inferred from the appearance of new peaks, while variations in the original functional groups can be inferred by changes in the signals of the parent functional groups.

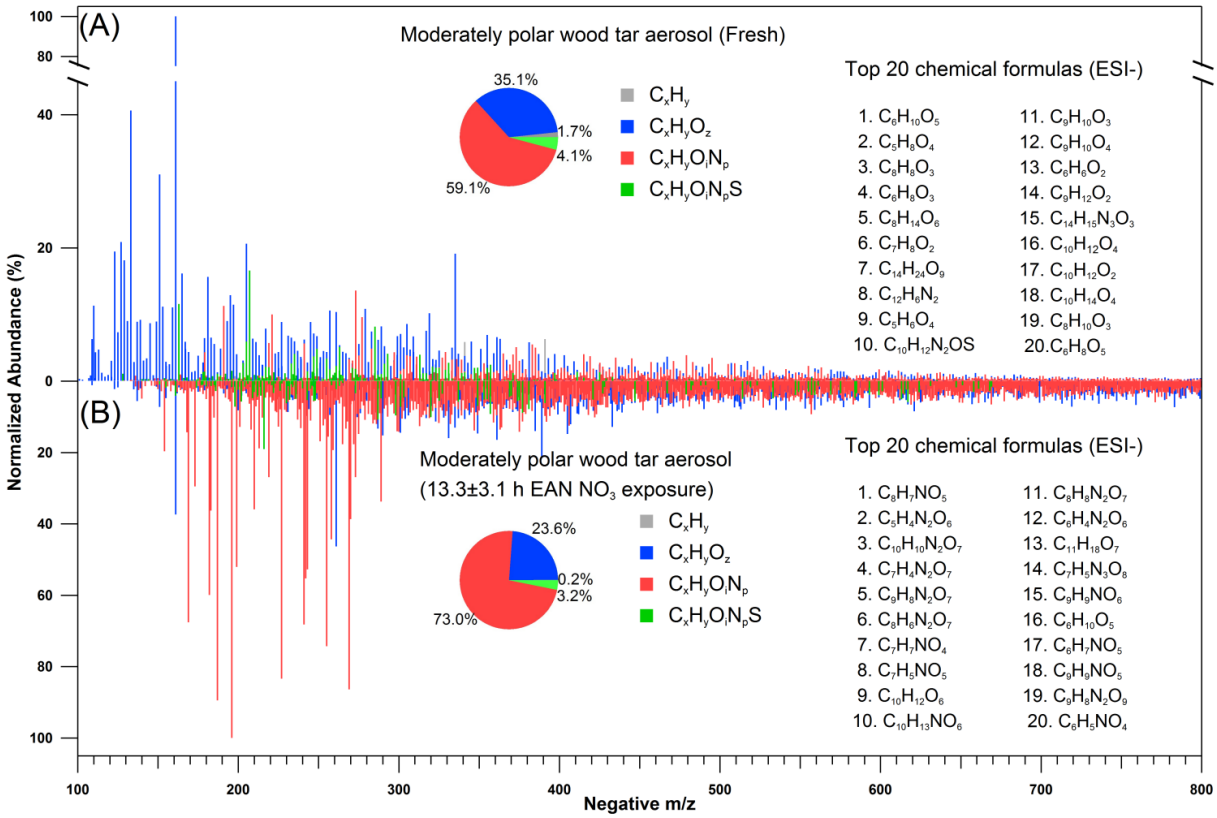

Figure S9. High-resolution negative ion mode mass spectra of moderately polar wood tar aerosol obtained before and after 13.3 h equivalent ambient NO_3 radial reaction. The spectra are normalized with respect to the highest intensity of identified molecule. Four chemical groups were classified based on their elemental compositions as C_xH_y, $C_xH_yO_z$, $C_xH_yO_iN_p$, $C_xH_yO_iN_pS$, where $x \geq 2$, $y \geq 2$, $z \geq 1$, $i \geq 0$, and $p \geq 0$, respectively. The relative contributions of the four parent chemical groups which constitute the skeletal for all the identified molecules. On the right, 20 identified molecular formulas, obtained with the highest intensity, are shown.

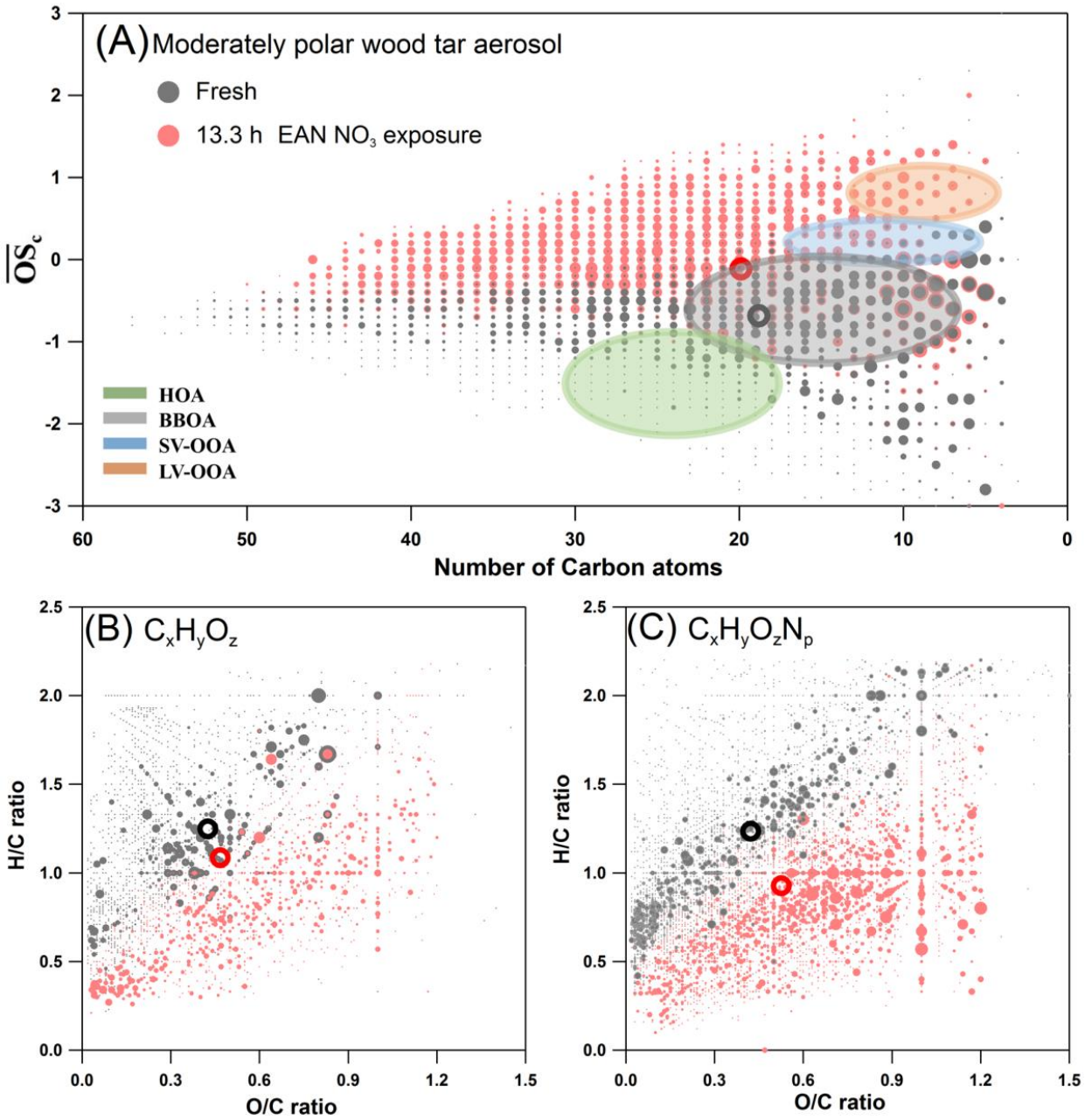

Figure S10. Comparison of molecular characteristics of moderately polar wood tar aerosol before and after 13.3 h of EAN NO_3 radial reaction. (A) carbon oxidation state ($\overline{OS}$≈2×O/C-H/C-5×N/C) as a function of molecular carbon number (n_C), (B)-(C) Van Krevelen plots of H/C and O/C ratios, for the identified molecule formula from direct infusion (-)ESI-HRMS measurement. The size of the dots indicates the relative intensity obtained for each molecular ion. Characteristic $\overline{OS}$-n_C for primarily emitted hydrocarbon-like organic aerosol (HOA) and biomass burning organic aerosol (BBOA) were located in light green and gray regions in (A), characteristic $\overline{OS}$-n_C for semivolatile and low-volatile organic aerosol (SV-OOA and LV-OOA) corresponded to "fresh" and "aged" secondary aerosol produced by secondary oxidation were grouped in light indigo and orange regions in (A).[44] Open dot was ion intensity weighted average elemental ratio corresponding to each group.

Table S6. Average elemental composition, elemental ratios, and carbon oxidation state ($\overline{OS}$) for moderately polar wood tar aerosol before and after 13.3 h equivalent ambient NO_3 radial reaction. Results were derived from (-) ESI-HRMS measurements.

Elemental characteristic	‹C›	‹H›	‹O›	‹N›	‹S›	‹H/C›	‹O/C›	‹N/C›	‹$\overline{OS}$›
Unprocessed	18.60	22.75	5.79	0.68	0.07	1.22	0.31	0.04	-0.80
NO_3 radical reacted	20.58	21.56	9.69	1.32	0.02	1.05	0.47	0.06	-0.41
difference	1.98	-1.19	3.90	0.64	-0.05	-0.17	0.16	0.02	0.39

Note: These signal intensity weighted average molecular information was obtained by assuming unified response of different compounds. However, different organic compounds might have different sensitivities in the (-) ESI-HRMS. Thus, uncertainties exist when we use the ion intensities for calculating average molecular information.

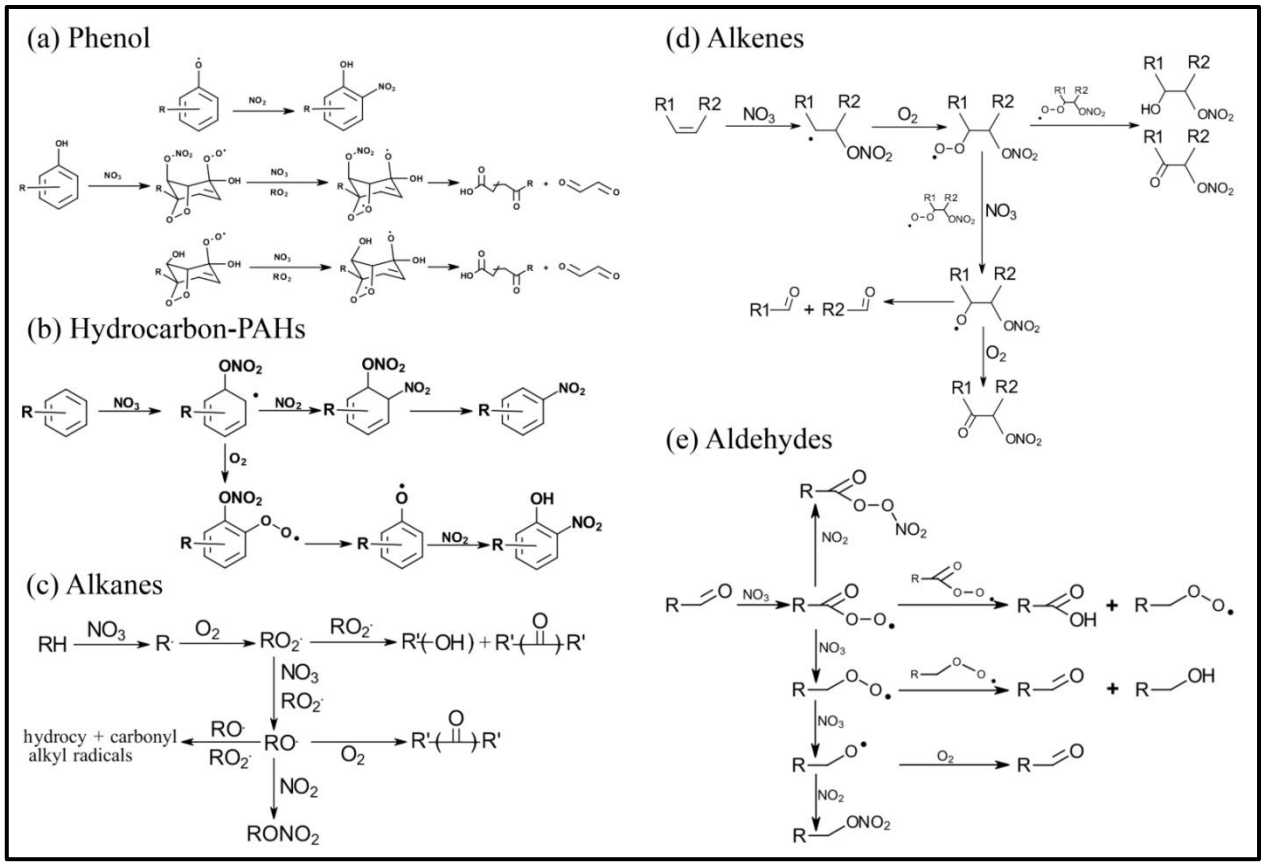

Figure S11. Proposed mechanism for NO_3 radical reactions of organic family that were identified in wood tar aerosols in presence of NO_2 and O_2 with organic family that were identified in wood tar aerosol. All schematic reaction pathways were extracted from MCM (http://mcm.leeds.ac.uk/MCMv3.3.1/roots.htt) and related publications,[23,35,45,46] only some main reaction pathways were included.

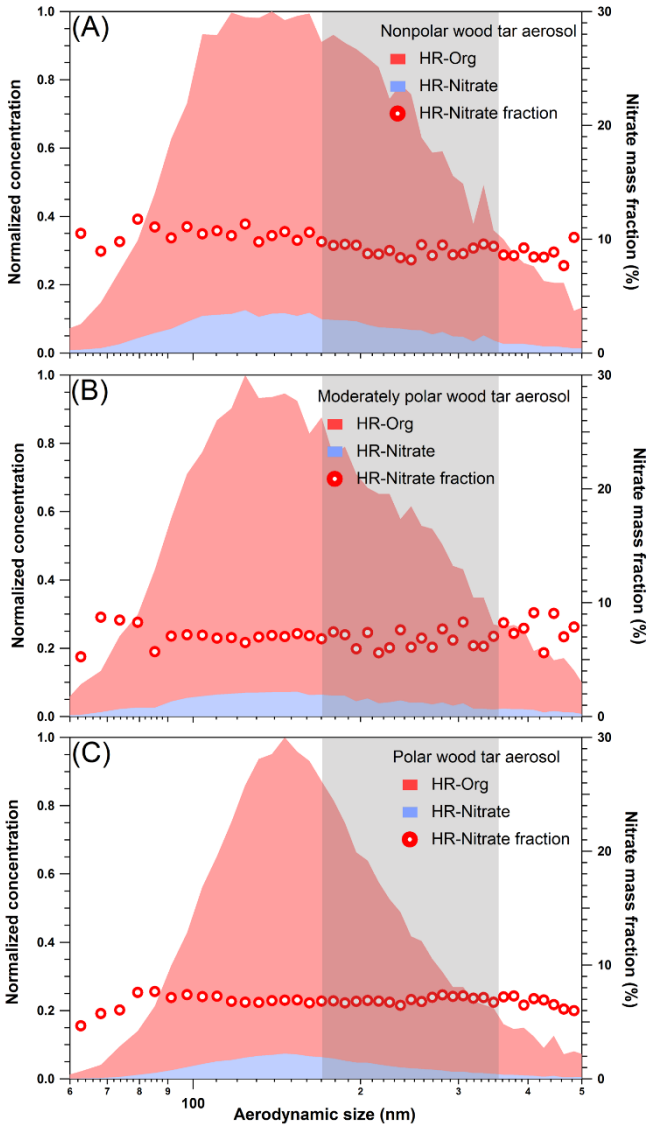

Figure S12. HR-Tof-AMS measured chemical composition and nitrate mass fraction as a function of particle size for NO_3 radical reacted wood tar aerosols (13.3 hr *EAN*).

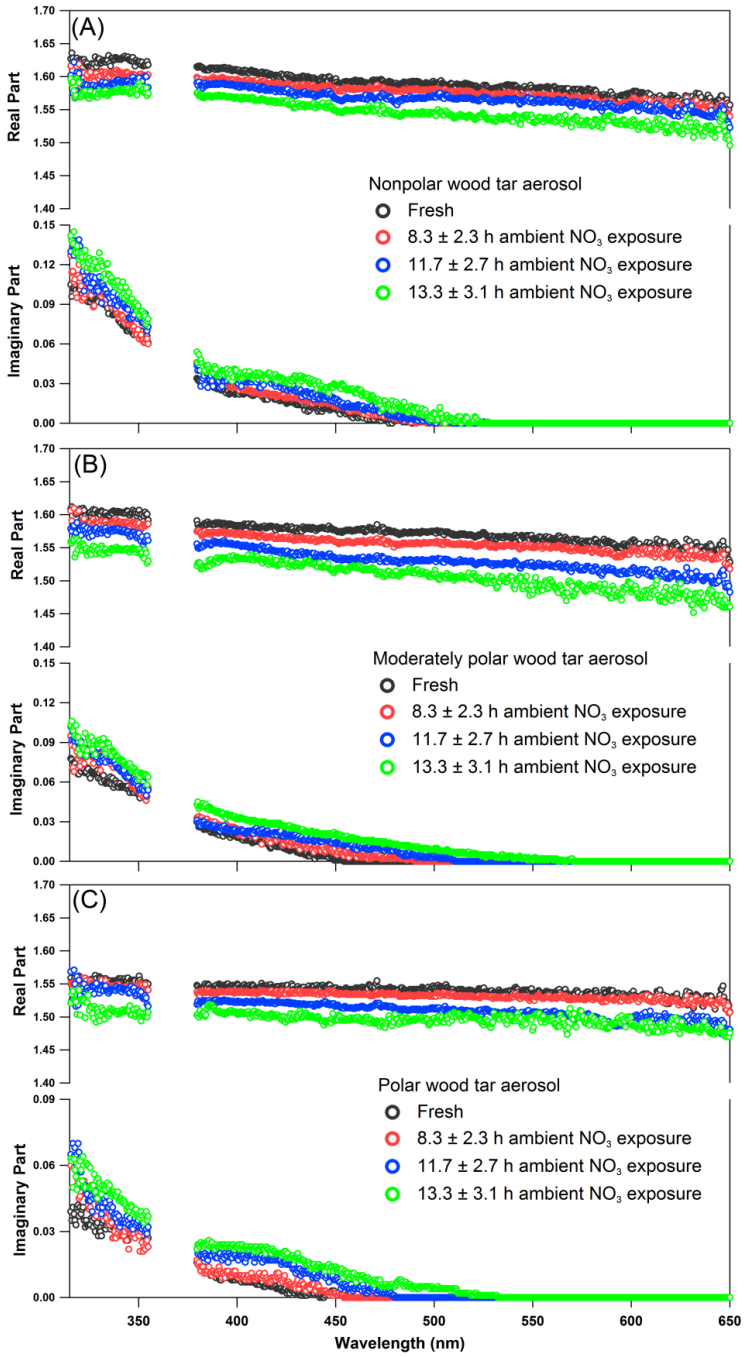

Figure S13. Retrieved broadband complex RIs as a function of wavelength (315-355 and 385-650 nm) and NO_3 radical aged degree (fresh to 13.3 hr equivalent field NO_3 radical oxidation at night) for: (A) nonpolar, (B) moderately polar, and (C) polar wood tar aerosols. For clarity, the error bar (±0.006 for real part and ±0.003 for imaginary part on average) for the retrieved RI are not shown, and can be found in the supporting information excel file.

References

(1) Tóth, A.; Hoffer, A.; Nyirő-Kósa, I.; Pósfai, M.; Gelencsér, A., Atmospheric tar balls: aged primary droplets from biomass burning? *Atmos. Chem. Phys.* **2014,** *14*, (13), 6669-6675.

(2) Li, C.; He, Q.; Schade, J.; Passig, J.; Zimmermann, R.; Laskin, A.; Rudich, Y., Dynamic changes of optical and chemical properties of tar ball aerosols by atmospheric photochemical aging. *Atmos. Chem. Phys.* **2019,** *2019*, (19), 139-163.

(3) He, Q.; Bluvshtein, N.; Segev, L.; Meidan, D.; Flores, J. M.; Brown, S. S.; Brune, W.; Rudich, Y., Evolution of the complex refractive index of secondary organic aerosols during atmospheric aging. *Environ. Sci. Technol.* **2018,** *52*, (6), 3456-3465.

(4) Riziq, A. A.; Rudich, Y., Progress in the investigation of aerosols' optical properties using cavity ring-down spectroscopy. *Fundamentals and Applications in Aerosol Spectroscopy* **2010**, 269.

(5) Berden, G.; Engeln, R., Cavity ring-down spectroscopy: techniques and applications. John Wiley & Sons: 2009.

(6) Brown, S.; Stark, H.; Ravishankara, A., Cavity ring-down spectroscopy for atmospheric trace gas detection: application to the nitrate radical (NO_3). *Appl. Phys. B* **2002,** *75*, (2-3), 173-182.

(7) Tavakoli, F.; Olfert, J. S., Determination of particle mass, effective density, mass-mobility exponent, and dynamic shape factor using an aerodynamic aerosol classifier and a differential mobility analyzer in tandem. *J. Aerosol Sci*. **2014,** *75*, 35-42.

(8) Tavakoli, F.; Olfert, J., An instrument for the classification of aerosols by particle relaxation time: theoretical models of the aerodynamic aerosol classifier. *Aerosol Sci. Technol.* **2013,** *47*, (8), 916-926.

(9) Nir Bluvshtein, J. M. F., Lior Segev, Yinon Rudich, A new approach for retrieving the UV-vis optical properties of ambient aerosols. *Atmos. Meas. Tech*. **2016,** *9*, (8), 3477.

(10) Washenfelder, R.; Flores, J.; Brock, C.; Brown, S.; Rudich, Y., Broadband measurements of aerosol extinction in the ultraviolet spectral region. *Atmos. Meas. Tech*. **2013,** *6*, (4), 861-877.

(11) Adler, G.; Riziq, A. A.; Erlick, C.; Rudich, Y., Effect of intrinsic organic carbon on the optical properties of fresh diesel soot. *Proc. Natl. Acad. Sci. U. S. A.* **2010,** *107*, (15), 6699-6704.

(12) Flores, J. M.; Trainic, M.; Borrmann, S.; Rudich, Y., Effective broadband refractive index retrieval by a white light optical particle counter. *Phys. Chem. Chem. Phys*. **2009,** *11*, (36), 7943-7950.

(13) Lu, J. W.; Flores, J. M.; Lavi, A.; Abo-Riziq, A.; Rudich, Y., Changes in the optical properties of benzo[a]pyrene-coated aerosols upon heterogeneous reactions with NO_2 and NO_3. *Phys. Chem. Chem. Phys*. **2011,** *13*, (14), 6484-6492.

(14) Aiken, A. C.; Decarlo, P. F.; Kroll, J. H.; Worsnop, D. R.; Huffman, J. A.; Docherty, K. S.; Ulbrich, I. M.; Mohr, C.; Kimmel, J. R.; Sueper, D., O/C and OM/OC ratios of primary, secondary, and ambient organic aerosols with high-resolution time-of-flight aerosol mass spectrometry. *Environ. Sci. Technol.* **2008,** *42*, (12), 4478-4485.

(15) Jennerwein, M.; Eschner, M.; Wilharm, T.; Gröger, T.; Zimmermann, R., Evaluation of reversed phase versus normal phase column combination for the quantitative analysis of common commercial available middle distillates using GC×GC-TOFMS and Visual Basic Script. *Fuel* **2019,** *235*, 336-338.

(16) Jennerwein, M. K.; Eschner, M. S.; Wilharm, T.; Zimmermann, R.; Gröger, T. M., Proof of concept of high-temperature comprehensive two-dimensional gas chromatography time-of-flight mass spectrometry for two-dimensional simulated distillation of crude oils. *Energy & Fuels* **2017,** *31*, (11), 11651-11659.

(17) Bae, E.; Yeo, I. J.; Jeong, B.; Shin, Y.; Shin, K.-H.; Kim, S., Study of double bond equivalents and the numbers of carbon and oxygen atom distribution of dissolved organic matter with negative-mode FT-ICR MS. *Anal. Chem.* **2011,** *83*, (11), 4193-4199.

(18) Laskin, J.; Laskin, A.; Roach, P. J.; Slysz, G. W.; Anderson, G. A.; Nizkorodov, S. A.; Bones, D. L.; Nguyen, L. Q., High-resolution desorption electrospray ionization mass spectrometry for chemical characterization of organic aerosols. *Anal. Chem.* **2010,** *82*, (5), 2048-2058.

(19) Lee, H. J.; Aiona, P. K.; Laskin, A.; Laskin, J.; Nizkorodov, S. A., Effect of solar radiation on the optical properties and molecular composition of laboratory proxies of atmospheric brown carbon. *Environ. Sci. Technol.* **2014,** *48*, (17), 10217-10226.

(20) Lin, P.; Aiona, P. K.; Li, Y.; Shiraiwa, M.; Laskin, J.; Nizkorodov, S. A.; Laskin, A., Molecular characterization of brown carbon in biomass burning aerosol particles. *Environ. Sci. Technol.* **2016,** *50*, (21), 11815-11824.

(21) Lin, P.; Fleming, L. T.; Nizkorodov, S. A.; Laskin, J.; Laskin, A., Comprehensive Molecular Characterization of Atmospheric Brown Carbon by High Resolution Mass Spectrometry with Electrospray and Atmospheric Pressure Photoionization. *Anal. Chem.* **2018**, 90, (21), 12493-12502.

(22) Gross, S.; Iannone, R.; Xiao, S.; Bertram, A. K., Reactive uptake studies of NO_3 and N_2O_5 on alkenoic acid, alkanoate, and polyalcohol substrates to probe nighttime aerosol chemistry. *Phys. Chem. Chem. Phys*. **2009,** *11*, (36), 7792-7803.

(23) Gross, S.; Bertram, A. K., Reactive uptake of NO_3, N_2O_5, NO_2, HNO_3, and O_3 on three types of polycyclic aromatic hydrocarbon surfaces. *J. Phys. Chem. A* **2008,** *112*, (14), 3104-3113.

(24) Chang, W. L.; Bhave, P. V.; Brown, S. S.; Riemer, N.; Stutz, J.; Dabdub, D., Heterogeneous atmospheric chemistry, ambient measurements, and model calculations of N_2O_5: A review. *Aerosol Sci. Technol.* **2011,** *45*, (6), 665-695.

(25) Ng, N. L.; Brown, S. S.; Archibald, A. T.; Atlas, E.; Cohen, R. C.; Crowley, J. N.; Day, D. A.; Donahue, N. M.; Fry, J. L.; Fuchs, H., Nitrate radicals and biogenic volatile organic compounds: oxidation, mechanisms, and organic aerosol. *Atmos. Chem. Phys.* **2017,** *17*, (3), 2103-2162.

(26) Phillips, G. J.; Thieser, J.; Tang, M.; Sobanski, N.; Schuster, G.; Fachinger, J.; Drewnick, F.; Borrmann, S.; Bingemer, H.; Lelieveld, J., Estimating N_2O_5 uptake coefficients using ambient measurements of NO_3, N_2O_5, $ClNO_2$ and particle-phase nitrate. *Atmos. Chem. Phys.* **2016**, 16, 13231-13249.

(27) Crowley, J.; Ammann, M.; Cox, R.; Hynes, R.; Jenkin, M. E.; Mellouki, A.; Rossi, M.; Troe, J.; Wallington, T., Evaluated kinetic and photochemical data for atmospheric chemistry: Volume V-heterogeneous reactions on solid substrates. *Atmos. Chem. Phys.* **2010,** *10*, (18), 9059-9223.

(28) Davidovits, P.; Kolb, C. E.; Williams, L. R.; Jayne, J. T.; Worsnop, D. R., Mass accommodation and chemical reactions at gas− liquid interfaces. *Chem. Rev.* **2006,** *106*, (4), 1323-1354.

(29) Pöschl, U.; Rudich, Y.; Ammann, M., Kinetic model framework for aerosol and cloud surface chemistry and gas-particle interactions-Part 1: General equations, parameters, and terminology. *Atmos. Chem. Phys.* **2007,** *7*, (23), 5989-6023.

(30) Ammann, M.; Pöschl, U., Kinetic model framework for aerosol and cloud surface chemistry and gas-particle interactions-Part 2: Exemplary practical applications and numerical simulations. *Atmos. Chem. Phys.* **2007,** *7*, (23), 6025-6045.

(31) Zasypkin, A. Y.; Grigor'eva, V.; Korchak, V.; Gershenson, Y. M., A formula for summing of kinetic resistances for mobile and stationary media: I. Cylindrical reactor. *Kinet. Cat.* **1997,** *38*, (6), 772-781.

(32) Knopf, D. A.; Forrester, S. M.; Slade, J. H., Heterogeneous oxidation kinetics of organic biomass burning aerosol surrogates by O_3, NO_2, N_2O_5, and NO_3. *Phys. Chem. Chem. Phys*. **2011,** *13*, (47), 21050-21062.

(33) Kolb, C.; Cox, R. A.; Abbatt, J.; Ammann, M.; Davis, E.; Donaldson, D.; Garrett, B. C.; George, C.; Griffiths, P.; Hanson, D., An overview of current issues in the uptake of atmospheric trace gases by aerosols and clouds. *Atmos. Chem. Phys.* **2010,** *10*, (21), 10561-10605.

(34) George, I.; Abbatt, J., Heterogeneous oxidation of atmospheric aerosol particles by gas-phase radicals. *Nat. Chem.* **2010,** *2*, (9), 713.

(35) Liu, C.; Zhang, P.; Wang, Y.; Yang, B.; Shu, J., Heterogeneous reactions of particulate methoxyphenols with NO3 radicals: Kinetics, products, and mechanisms. *Environ. Sci. Technol.* **2012,** *46*, (24), 13262-13269.

(36) Shiraiwa, M.; Pöschl, U.; Knopf, D. A., Multiphase chemical kinetics of NO_3 radicals reacting with organic aerosol components from biomass burning. *Environ. Sci. Technol.* **2012,** *46*, (12), 6630-6636.

(37) Tang, M.; Cox, R.; Kalberer, M., Compilation and evaluation of gas phase diffusion coefficients of reactive trace gases in the atmosphere: volume 1. Inorganic compounds. *Atmos. Chem. Phys.* **2014,** *14*, (17), 9233-9247.

(38) Li, H.; Zhu, T.; Zhao, D.; Zhang, Z.; Chen, Z., Kinetics and mechanisms of heterogeneous reaction of NO_2 on $CaCO_3$ surfaces under dry and wet conditions. *Atmos. Chem. Phys.* **2010,** *10*, (2), 463-474.

(39) Khan, M.; Cooke, M.; Utembe, S.; Archibald, A.; Derwent, R.; Xiao, P.; Percival, C.; Jenkin, M.; Morris, W.; Shallcross, D., Global modeling of the nitrate radical (NO_3) for present and pre-industrial scenarios. *Atmos. Res.* **2015,** *164*, 347-357.

(40) Asaf, D.; Tas, E.; Pedersen, D.; Peleg, M.; Luria, M., Long-term measurements of NO_3 radical at a semiarid urban site: 2. Seasonal trends and loss mechanisms. *Environ. Sci. Technol.* **2010,** *44*, (15), 5901-5907.

(41) Decker, Z.; Zarzana, K.; Coggon, M. M.; Min, K.-E.; Pollack, I.; Ryerson, T. B.; Peischl, J.; Edwards, P.; Dubé, W. P.; Markovic, M. Z., Nighttime chemical transformation in biomass burning plumes: a box model analysis initialized with aircraft observations. *Environ. Sci. Technol.* **2019**, 53, (5), 2529-2538.

(42) Brown, S. S.; Stutz, J., Nighttime radical observations and chemistry. *Chem. Soc. Rev.* **2012,** *41*, (19), 6405-6447.

(43) Bluvshtein, N.; Lin, P.; Flores, J. M.; Segev, L.; Mazar, Y.; Tas, E.; Snider, G.; Weagle, C.; Brown, S. S.; Laskin, A., Broadband optical properties of biomass-burning aerosol and identification of brown carbon chromophores. *J. Geophys. Res.: Atmos.* **2017**, 122, 5441-5456. DOI: 10.1002/2016JD026230.

(44) Kroll, J. H.; Donahue, N. M.; Jimenez, J. L.; Kessler, S. H.; Canagaratna, M. R.; Wilson, K. R.; Altieri, K. E.; Mazzoleni, L. R.; Wozniak, A. S.; Bluhm, H., Carbon oxidation state as a metric for describing the chemistry of atmospheric organic aerosol. *Nat. Chem.* **2011,** *3*, (2), 133.

(45) Gross, S.; Bertram, A. K., Products and kinetics of the reactions of an alkane monolayer and a terminal alkene monolayer with NO_3 radicals. *J. Geophys. Res.: Atmos*. **2009,** *114*, (D02307), 1-14. DOI: 10.1029/2008JD010987.

(46) Docherty, K. S.; Ziemann, P. J., Reaction of oleic acid particles with NO_3 radicals: Products, mechanism, and implications for radical-initiated organic aerosol oxidation. *J. Phys. Chem. A* **2006,** *110*, (10), 3567-3577.